Human receptive endometrial assembloid for deciphering the implantation window

Yu Zhang[acdef*], Rusong Zhao[abcdefgh*], Chaoyan Yang[acdef], Jinzhu Song[acdef], Peishu Liu[i], Yan Li[acdefgh], Boyang Liu[acdefgh], Tao Li[jk], Changjian Yin[acdef], Minghui Lu[acdef], Zhenzhen Hou[acdef], Chuanxin Zhang[acdef], Zi-Jiang Chen[acdefghlm#], Keliang Wu[acdefgh#], Han Zhao[acdefgh#]

Author affiliation:

a. State Key Laboratory of Reproductive Medicine and Offspring Health, Center for Reproductive Medicine, Institute of Women, Children and Reproductive Health, Cheeloo College of Medicine, Shandong University, 250012, China

b. The Affiliated Suzhou Hospital of Nanjing Medical University, Suzhou Municipal Hospital, Gusu School, Nanjing Medical University, Suzhou, Jiangsu, 215000, China

c. National Research Center for Assisted Reproductive Technology and Reproductive Genetics, Shandong University, Jinan, Shandong, 250012, China

d. Key Laboratory of Reproductive Endocrinology (Shandong University), Ministry of Education, Jinan, Shandong, 250012, China

e. Shandong Technology Innovation Center for Reproductive Health, Jinan, Shandong, 250012, China

f. Shandong Provincial Clinical Research Center for Reproductive Health, Jinan, Shandong, 250012, China

g. Shandong Key Laboratory of Reproductive Medicine, Shandong Provincial Hospital Affiliated to Shandong First Medical University, Jinan, Shandong, 250012, China

h. Research Unit of Gametogenesis and Health of ART-Offspring, Chinese Academy of Medical Sciences (No.2021RU001), Jinan, Shandong, 250012, China

i. Department of Obstetrics and Gynecology, Qilu Hospital of Shandong University, Jinan, Shandong, 250012, China

j. Department of Gynecology, Shandong Provincial Hospital, Cheeloo College of Medicine, Shandong University, Jinan, Shandong, 250021, China.

k. Department of Gynecology, Shandong Provincial Hospital Affiliated to Shandong First Medical University, Jinan, Shandong, 250021, China

l. Shanghai Key Laboratory for Assisted Reproduction and Reproductive Genetics, Shanghai, 200135, China

m. Department of Reproductive Medicine, Ren Ji Hospital, Shanghai Jiao Tong University School of Medicine, Shanghai, 200135, China

*These authors contributed equally: Yu Zhang, Rusong Zhao.

#To whom correspondence may be addressed. Email: hanzh80@sdu.edu.cn, wukeliang_527@163.com, chenzijiang@hotmail.com

Classifications: Cell Biology

Abstract

Human endometrial receptivity is a critical determinant of pregnancy success; however, in vivo studies of its features and regulation are particularly challenging due to ethical restriction. Recently, the development of human endometrial assembloids has provided a powerful model to examine this intricate biological process. In this study, we established a specialized human window-of-implantation (WOI) endometrial assembloid system that mimics the in vivo receptive endometrium. It recapitulates not only the structural attributes of pinopodes and cilia, but also molecular characteristics of mid secretory endometrium. Furthermore, the WOI endometrial assembloid exhibits hormone responsiveness, energy metabolism with larger and enhanced functional mitochondria, increased ciliary assembly and motility, and epithelial-mesenchymal transition (EMT), as well as promising potential for embryo implantation. As such, WOI assembloids hold great promise as a platform to unravel the intricate mechanisms governing endometrial receptivity regulation, maternal-fetal interactions, and associated diseases, ultimately driving impactful advancements in the field.

Keywords

Endometrium, assembloid, implantation window

Introduction

The human endometrium, comprising various cell types, experiences shedding (menstrual phase), regeneration (proliferative phase), and differentiation (secretory phase) under the regulation of estrogen and progesterone during the menstrual cycle (1). A brief window, called the "window-of-implantation (WOI)" or mid-secretory phase, allows for embryo implantation into the endometrium (1). The endometrium at the embryo implantation site contains diverse cells, including ciliated epithelial cells, decidualized stromal cells and immune cells. Cyclic endometrial changes akin to those in humans are exclusive to apes, Old World monkeys, molossid bats, and spiny mice, but not mice (1), rendering typical mouse models insufficient for accurately simulating human endometrium. Existing endometrial cell lines, such as Ishikawa and HEEC cells, consist solely of a single cell type, thus failing to reproduce the intricate physiological structure and function of the endometrium.

Replicating and reconstructing human organs has become essential for exploring tissue physiology and function. O rganoid, a self-assembled 3D structure, closely resemble in vivo tissue or organ (2). They offer high expansibility, phenotypic, and functional properties, emerging as powerful tools for investigating tissue physiology and disease (3). In 2017, the first long-term and hormone-responsive human endometrial organoid was established using adult stem cells from endometrial biopsy(2, 3). Based on this, Margherita Y. Turco, et al developed noninvasive methods to construct endometrial organoids from menstrual flow(4). Takahiro Arima et al. developed polar reversal endometrial organoids to study embryo implantation(5). Apart from adult stem cells, pluripotent stem cells were also induced to endometrial stromal fibroblasts and epithelium, and then cocultured to form organoids(6, 7), which offered vigorous proliferative capacity but lacked immune cells and other components of the microenvironment. There are also studies that add immune cells to endometrial organoids for co-culture(8). In efforts to mimic human endometrial cell types in vitro, the endometrial organoids progressed from epithelial organoids(9), to assemblies of epithelial and stromal cells(10, 11) and then to stem cell-laden 3D artificial endometrium(12, 13), which were solely closer but not completely identical to the endometrium. Additionally, pathological endometrial organoid models have been established for conditions like endometriosis, endometrial hyperplasia, Lynch syndrome, and endometrial cancer (14). These organoids simulated

endometrial morphology, hormone responsiveness, and physiological and pathological processes in vitro (3, 9, 15-17), facilitating the study of physiological phenomena (15, 18, 19), pathogenic mechanisms(16) and drug screening(14).

Although various regulators have been suggested to be involved in WOI, we are far from understanding how embryo implantation occurs during the WOI due to ethical limitations and fewer in vitro receptive endometrial model. Transforming from proliferative to receptive endometrium involves dynamic changes like decidualization, epithelial-mesenchymal transition (EMT) and ciliated epithelial development (1, 20), which have not been reconstructed in most in vitro model to date. Here, we successfully established a receptive endometrial assembloid system regulated by hormones and reflecting the in vivo WOI endometrial features, providing a platform for studying physiological and pathological endometrium and maternal-fetal interactions.

Results

Developing receptive endometrial assembloids in vitro

To establish endometrial assembloids in vitro, pre-receptive endometrium from reproductive-age women was dissociated into single cells or small cell masses. These cells then self-assembled into assembloids induced by various small molecules, such as Noggin, EGF, FGF2, WNT-3A and R-Spondin1 in expansion medium (ExM) (Fig.1A~B, Fig.S1A). The assembloids derived from the first generation are used for experiments (Fig.S1B). The endometrial assembloids consist of vesicle-like glands and fibrous stromal cells (Fig. S1C, Video S1~S4). The epithelium marker E-cadherin, stromal cell marker vimentin, and endometrial gland marker FOXA2 were expressed in the cultured endometrial assembloid, which resembled the endometrium morphologically (Fig. S1D). Moreover, the endometrial assembloids exhibited substantial expression of the proliferation marker Ki67, while the apoptosis marker cleaved caspase-3 was undetectable, signifying the assembloids' robust proliferative capacity (Fig. S1E).

Functionally, endometrial assembloids effectively secreted glycogen into the lumen, mirroring the in vivo endometrial activity, thereby providing nourishment for embryo implantation (Fig. S1D). Moreover, after two days of estrogen (E2) treatment followed by fourteen days of medroxyprogesterone acetate (MPA) and cAMP administration, the assembloids exhibited a significant upregulation of progesterone receptor (PRA/B) expression, a modest increase in estrogen receptor α (ERα), and enhanced expression of estrogen-responsive genes *EGR1* and *OLFM4*, along with progesterone-responsive genes *PGR* and *PAEP* at the transcriptional level (Fig. S1F~S1G). It reflected a comparable hormonal responsiveness in the in vivo endometrium.

To identify hormonal regimens that induce implantation window, pregnancy-related hormones were supplemented into the culture system following the two-day E2. E2 and MPA promote the transition of endometrial assembloids into the secretory phase, while pregnancy hormones can promote the further differentiation. Prolactin (PRL) promotes immune regulation and angiogenesis during implantation(2, 21). Human chorionic gonadotropin (hCG) improves endometrial thickness and receptivity (22, 23). Human placental lactogen (hPL) promotes the development and function of endometrial glands(24). Hormone dosage was primarily based on peri-pregnant maternal body or localized endometrium levels (2). A comparison of multiple groups revealed similar counts, area,

and average intensity of assembloids over time (Fig.1C-D, Fig.S1H). However, only the final recipe (i.e., a combination of E2, MPA, cAMP, PRL, hCG and hPL) exhibited an endometrial receptivity-related gene expression profile, which highly expressed genes positively correlated with endometrial receptivity, and lowly expressed genes negatively correlated with receptivity, compared to the other hormone formulations (Fig.1E). The assembloids induced with this scheme were defined as WOI assembloids (Fig. 1A). In contrast, endometrial assembloids maintained in ExM constituted the "control (CTRL)" group, whereas assembloids treated with E2 for two days, followed by E2, MPA, and cAMP for an additional six days, were induced to the secretory phase as previously reported(9), and designated as the "secretory (SEC)" group (Fig. 1A). There was no significant difference in the morphology of assembloids among the three groups (Fig.1B), but when comparing receptivity markers, WOI assembloids exhibited high expression of IGFBP1, MAOA, and DPP4 (Fig. 1F), with increased glycogen secretion (Fig.S1I). Theoretically, the WOI assembloids are initially in the secretory phase, thus sharing characteristics with the SEC assembloids. More importantly, they are expected to display traits typical of the mid-secretory phase.

Receptive endometrial assembloids mimicked the implantation - window endometrium

Single-cell transcriptomics analysis identified the presence of epithelium, stromal cells, and immune cells in WOI assembloids with reference to CellMarker, PanglaoDB, Human Cell Atlas, Human Cell Landscape, and scRNASeqDB, and previous endometrium related studies(1, 9, 11, 25) (Fig. 2A, Fig. S2A~S2B). The WOI assembloids exhibited similarities to the mid-secretory endometrium in terms of glandular and luminal epithelium, secretory epithelium, LGR5 epithelium, ciliated epithelium, and EMT-derived cells, as evidenced by comparisons of scRNA-seq data from our assembloids and the mid-secretory endometrium as described by Stephen R. Quake in 2020 (1) (Fig.2A, Fig.S2C~S2D). The morphology of immune and stromal cells was analyzed through 3D clearing staining and light sheet microscopy imaging, with vimentin labeling stromal cells (Vimentin^{+} or Vimentin^{+} F-actin^{+}), CD45 and CD44 indicating immune cells, and FOXA2 identifying glands (Fig.2B~2D). Furtherly, we confirmed the presence and types of immune cells using flow cytometry. White blood cells (WBC) were identified as CD45^{+} cells, with T cells,

macrophages and NK cells characterized as $CD45^+CD3^+$ cells, $CD45^+CD68^+CD11b^+$ cells and $CD56^+CD16^-$ cells, respectively (Fig. 2E).

The WOI assembloids displayed characteristic features of the receptive endometrium. On the one hand, the WOI assembloids secreted more glycogen into the lumen (Fig. S1I). On the other hand, the WOI assembloids possessed various characteristic microstructure of implantation window, including elongated microvilli and increased glycogen, pinopodes, and especially cilia (Fig.2F).

Further, we concentrated on the comparison of gene expression and transcriptional regulation during the mid-secretory phase, as this phase marks the implantation window and involves substantial transcriptional alterations (Fig.2G~2H). We referred to the scRNA-seq data of the mid-secretory phase from Stephen R. Quake 2020 (1). Pathways related to mitochondrial energy metabolism and cell adhesion exhibited upregulation in both the WOI assembloid and mid-secretory endometrium in comparison to the CTRL and SEC assembloids (Fig. 2G). The crucial transcription factors (TFs) found in the secretory epithelium and EMT-derived cells, which are implicated in implantation, revealed similarities between WOI assembloids and mid-secretory endometrium. Specifically, the secretory epithelium exhibited comparable TFs related to hypoxia response (such as previously reported HIF1A(26)), embryo implantation (such as FBLN1(27)), lipid metabolism (such as VMP1(28)), cell migration, and cell junction (such as TJP1(29)) (Fig. 2H). Similarly, EMT-derived cells also expressed similar TFs involved in endometrial decidualization (such as S100A10(30)), EMT (such as FAT1(31) and FOXF2(32)), and receptivity (such as NEAT1(33), SERPINB9(34), SOX17(35) and SOX4(36)) (Fig. 2H).

We then conducted the endometrial receptivity test (ERT) (37) to further assess the receptive state of WOI assembloids. ERT is a kind of gene analysis-based method for detecting endometrial receptivity, which combines high-throughput sequencing and machine learning to analyze the expression of endometrial receptivity-related genes (37). It is currently used in clinical practice to determine endometrial receptivity and guide personalized embryo transfer. The WOI assembloids derived from pre-receptive endometrium were observed to transit into the receptivity phase (Fig. S1J).

Collectively, these results demonstrated that the WOI assembloids closely resemble the in vivo endometrium during the implantation window in terms of structures and molecular characteristics.

Receptive endometrial assembloids recapitulate WOI-associated hormone response

We analyzed the transcriptome and proteome profiles of WOI assembloids compared to those of CTRL or SEC assembloids to assess WOI associated biological characteristics (Fig. 3A, Fig. S3A~S3E).

WOI assembloids exhibited a robust hormone response, as demonstrated by the upregulation of PGR at the transcriptome level (Fig. 3B). Integrated analysis of the transcriptome and proteome data identified 179 upregulated genes/proteins in WOI assembloids compared to the CTRL group, with most of these genes/proteins implicated in the estrogen response (Fig. S3F~S3G). Furthermore, the analysis of progesterone response levels using PRA/B immunostaining indicated the highest levels in the WOI group, accompanied by an upregulation of the estrogen responsive protein OLFM4 (Fig. 3C). FOXO1, a crucial marker of endometrial receptivity reliant on PGR signaling, exhibited significantly elevated expression in WOI assembloids compared to CTRL assembloids (Fig.3D, Video S5), suggesting the involvement of progesterone signaling in the establishment of WOI assembloids. These findings collectively demonstrated a strong response of WOI assembloids to estrogen and progesterone.

Hormone response increased secretory epithelium and decreased proliferative epithelium in the SEC and WOI assembloids, suggesting the transformation from proliferation to secretory phase (Fig. 3E). The secretory epithelium, critical for the implantation window, contributed to cellular metabolic processes and HIF-1 signaling pathway response to hypoxia at the single-cell level (Fig. S2E~S2F). The secretory epithelium of WOI assembloids exhibited enhanced peptide metabolism and mitochondrial energy metabolism compared to the SEC group, supporting endometrial decidualization and embryo implantation (Fig. 3F). Proliferative epithelium differentiates into secretory epithelium under the regulation of branch nodal genes between state 5 and state 6, such as the KRT19, MALAT1, MT2A, RPL and RPS families, as revealed by single-cell trajectory (Fig. 3G, Fig. S2H~S2J). The WOI assembloids showed more thoroughly differentiation from proliferative to secretory epithelium in relation to the SEC assembloids (Fig. 3G).

Overall, the WOI assembloids possessed the hormone response characteristic of implantation window, closely resembling the gene traits of embryo implantation.

Receptive endometrial assembloids possess enhanced energy metabolism

The WOI assembloids exhibited upregulation of monocarboxylic acid and lipid metabolism (represented by SLC25A1(38)), and hypoxia response (represented by HIF1α(26)) (Fig.3B, Fig.S3G~S3I). Likewise, the secretory epithelium, critical for the implantation window, contributed to cellular metabolic processes and HIF-1 signaling pathway response to hypoxia at the single-cell level (Fig. S2E~S2F).

To further investigate this trend, the Mfuzz algorithm was utilized to analyze gene expression across these three groups, focusing on gene clusters that were progressively upregulated or downregulated. It was observed that mitochondrial genes exhibited the highest expression levels in WOI endometrial assembloids (Fig. 4A). Additionally, at the protein level, WOI endometrial assembloids showed sustained high expression of mitochondrial proteins compared to SEC assembloids (Fig. 4B). TEM analysis revealed that WOI endometrial assembloids had the largest average mitochondrial area (Fig. 4C). The expression of mitochondrial-related genes increased from CTRL to SEC to WOI assembloids, with COA1 ensuring proper nuclear-mitochondrial connection(39), OXA1L promoting mitochondrial translation(40), and TIMMDC1 being crucial for mitochondrial complex I assembly(41) (Fig. 4D). The WOI assembloids notably expressed higher levels of OXA1L and TIMMDC1 than the SEC assembloids (Fig. 4D). Furthermore, WOI assembloids produced more ATP and IL8(42) (Fig. 4E).

Thus, compared to SEC assembloids, WOI assembloids exhibited increased energy metabolism with larger and enhanced functional mitochondria.

Receptive endometrial assembloids increased the ciliary assembly and motility

The growth and development, assembly and movement of cilia, a characteristic endometrial structure, are essential for the establishment of endometrial implantation window and embryo implantation. Under the electron microscopy, the cilia were most observed in the WOI assembloids (Fig. 2E). Cilia-related genes and proteins exhibited the highest expression levels in WOI endometrial assembloids (Fig. 5A~5B). Compared to SEC assembloids, WOI endometrial assembloids showed upregulation in ciliary assembly, ciliary basal body, and motile cilia-related gene expressions, while genes related to non-motile cilia were downregulated (Fig. 5A).

Transcriptomic analysis further confirmed the upregulation of genes involved in ciliary assembly (*NEK2*), ciliary basal body (*CFAP36*), and motile cilia (*DNAH9 and TPPP*) in WOI endometrial assembloids, with *NEK2* showing the most significant difference (Fig.5B). Meanwhile, expressions of proteins related to ciliary assembly, ciliary basal body, and motile cilia were also increased in WOI assembloids, with the most notable differences observed in TBC1D1, IFT22, and IFT57 (ciliary assembly), and PJA2 (ciliary basal body) (Fig. 5C). Acetyl-α-tubulin (cilia marker (15)) were highly expressed in the WOI assembloids (Fig. 5D).

Single-cell transcriptome analysis revealed hormone treatment increased ciliated epithelium and decreased unciliated epithelium in SEC and WOI groups (Fig. 3E). Ciliated epithelium functioned in protein binding, cilium organization and assembly, while unciliated epithelium acted on actin cytoskeleton and translation (Fig. S2E~F). The WOI assembloids' ciliated epithelium regulated vasculature development and displayed higher transcriptional activity than the SEC group (Fig. 5E). Ciliated-unciliated epithelium transition occurred during the menstrual cycle, which was regulated by key genes, such as GAS5, JUN, RPL and RPS families (Fig. 5F, Fig.S2K~S2M). The implementation of aforementioned functions depended on its interaction with other cells. CellPhoneDB is a useful tool to investigate ligand-receptor interactions between the cells(43). Ciliated epithelium of WOI assembloids interacted with immune cells and secretory epithelium, showing enhanced invasion ability via CD74-COPA(44), and ROR2-WNT5A(45), which was validated by proximity ligation assay (PLA) (Fig. 5G~5H).

In summary, the WOI assembloids revealed accumulated ciliated epithelium's role in preparing the implantation window, with increased ciliary assembly and motility compared to SEC assembloids.

Receptive endometrial assembloids experienced epithelial-mesenchymal transition (EMT)

The WOI assembloids displayed upregulated cell differentiation not only at assembloid level (Fig. 3B) but also at cellular level, which is represented by EMT. EMT is a common and crucial biological event in the endometrium during the implantation window(46). During the EMT process, epithelial cells lose their epithelial characteristics while gaining migratory and invasive properties of fibroblasts. Synthetic analysis of the transcriptome and proteome revealed increased EMT in WOI assembloids (Fig. S3G).

EMT-derived cells, exhibiting gene expression patterns typical of epithelial and stromal cells, as well as EMT, are more abundant in the SEC and WOI groups, and act on protein binding, cell cycle, organelle organization, and reproduction (Fig. S2E). They performed enhanced lamellipodium-mediated cell migration, cell junction and cytoskeleton regulation in the WOI assembloids compared to the SEC assembloids (Fig. S4A). The WOI assembloids exhibited more thoroughly differentiation from proliferative epithelium to EMT-derived cells than the SEC assembloids, which was regulated by key genes such as DOC2B, FXYD3, and LPCAT3 (Fig. S4B~S4D). EMT-derived cells and epithelium cooperated during the implantation window (Fig. S4E). We found that NRP1 and SLC7A1 were highly expressed by EMT-derived cells, and their receptors (SEMA3A and CSF1) were more upregulated in the epithelium of WOI group than SEC group (Fig. S4E, S4G). NRP1-SEMA3A has been reported to promote vascularization and responds to hypoxia(47). SLC7A1(48) and CSF1(49) both support receptivity establishment, embryo implantation and development. Compared with common stromal cells, EMT-derived cells communicate slightly differently with epithelial or immune cells. CD44 and CD46, known for their roles in cell adhesion (51) and immunoregulation(52), are highly expressed in stromal cells and EMT-derived cells, respectively, and bind separately with SPP1 and JAG1 in epithelial and stromal cells (Fig. S4E~S4G).

In general, WOI assembloids demonstrated EMT's role in mediating endometrial transformation towards the implantation window.

The receptive endometrial assembloids possess the potential for embryo implantation

We further investigated the key biological function of the implantation window, specifically embryo implantation, using the assembloids. Given the rarity and ethical constraints associated with human embryos, we employed blastoids (corresponding to the human embryo at 6 days post-fertilization, referred to as "Day 6") for implantation into the endometrial assembloids (Fig.6A). By Day 9, we observed that the blastoids could grow within the endometrial assembloids and interact with them (Fig.6B). The co-cultured blastoids displayed normal tri-lineage differentiation, characterized by markers for the epiblast (OCT4), hypoblast (GATA6), and trophoblast (KRT18) (Fig.6C). Additionally, we conducted a comparative analysis of the survival rates of blastoids and their interaction rates with endometrial assembloids across the CTRL, SEC and WOI assembloids.

Remarkably, the survival and interaction rates of blastoids in the WOI endometrial assembloids were significantly higher compared to the CTRL and SEC groups, with survival rates of 66%, 19%, and 28%, and interaction rates of 90%, 47%, and 53% respectively, indicating the promising potential for embryo implantation (Fig.6D~E). This demonstrates that we have provided an innovative and supportive model suitable for embryo implantation.

In summary, WOI endometrial assembloids not only exhibited the typical structural and molecular features of the implantation window but also demonstrated significant potential for embryo implantation.

Discussion

In our study, we constructed the WOI endometrial assembloids, and observed the remarkable resemblance in structure and function to the in vivo endometrium. The assembloids consist of three primary types of endometrial cells, specifically epithelial, stromal, and immune cells, with epithelial cells assembling into glands and surrounded by immune cells and stromal cells. This similarity in cellular composition and tissue architecture to the endometrium lays the foundation for simulating receptive endometrium.

Although previous studies treated endometrial assembloid with E2, P4, and cAMP to induce a transition to the secretory phase, the methodology to accurately simulate the implantation window or mid-secretory endometrium remains elusive and warrants further investigation. Previous research suggested that placental signals could further promote the differentiation of endometrial assembloids (2), and PRL, hCG and HPL have been implicated in processes such as decidualization, implantation, immunoregulation, and angiogenesis (21, 22, 24). Detailly, PRL, synthesized by the adenohypophysis, endometrium, and myometrium, plays a vital role in implantation, immunoregulation, and angiogenesis, with the secretory endometrium producing PRL in response to MPA and E2, leading to ciliated cell formation and stromal cell decidualization (2, 21). HCG, secreted by trophoblasts in early pregnancy, influences decidual cells (22) and improves endometrial thickness and receptivity(23). The introduction of hCG has been shown to elevate the expression of critical factors associated with endometrial receptivity, such as endocytosis proteins, hypoxia-inducible factor 1 (HIF1), chemokines, and glycodelin (53). HPL contributes to the development and function of uterine glands(24). Consequently, the additional supplementation of PRL, hCG and HPL in our system augmented hormone responsiveness and receptivity, while promoting cell differentiation, ultimately yielding a model more representative of the receptive endometrium.

Here, the WOI assembloid exhibited the characteristic ultra-structures, such as cilia. During the human menstrual cycle, motile cilia are present in the epithelium of the endometrium(1). These hair-like organelles extend from the cell surface and beat rhythmically, facilitating cell and tissue movement while driving fluid transport across the epithelium (54). During the decidualization of the endometrium, the number and length of cilia increase, a process driven by the two primary

regulatory factors for embryo implantation: estrogen and progesterone (15, 55, 56). However, with aging, the expression of cilia-related genes in the endometrium is downregulated(57). In patients with recurrent implantation failure (RIF), ciliary defects in the endometrium are observed, leading to abnormal decidualization and repeated implantation failure(56). Thus, cilia play a crucial role in endometrial decidualization and embryo implantation. Consistently, the WOI assembloid exhibited increased ciliated epithelium, along with enhanced assembly and motility of cilia.

Furthermore, the WOI assembloid demonstrated energy and lipid metabolism patterns resembling those of the in vivo receptive endometrium. Enhanced energy metabolism involves monocarboxylic acid metabolism and mitochondrial oxidative phosphorylation. Monocarboxylic acids, exemplified by lactate, pyruvate, and ketone bodies, are vital metabolites in most mammalian cells. During the implantation window, elevated lactate levels mobilize endometrial monocarboxylic acid metabolism and function as a pregnancy-related signal, stimulating secretion in the epithelium. Subsequently, ATP, the primary product of energy metabolism, induces neighboring epithelial cells to release IL8, promoting decidualization of stromal cells (42). It was also observed that WOI assembloids indeed possessed larger and functionally active mitochondria, producing much more ATP and IL8 than CTRL and SEC assembloids. Lipid metabolism, responsible for energy storage, signal transduction, cell proliferation, apoptosis, and membrane trafficking, plays a crucial role in endometrial receptivity and implantation, although the precise mechanisms are not fully understood (58-60). Thus, the WOI assembloids possessed metabolic characteristics of in vivo implantation window.

However, our WOI endometrial assembloids also exhibit some limitations. It is undeniable that the assembloids cannot perfectly replicate the in vivo endometrium, which comprises functional and basal layers with a greater abundance of cell subtypes, under superior regulation by systemic hormones and nutrients. Stromal cells and immune cells are difficult to pass down stably and their proportion is lower than that in the in vivo endometrium. We are looking forward to combining stem cell induction, 3D printing technology, and microfluidic systems to alter the culture environment in order to optimize the existing model.

In summary, we developed a receptive endometrial assembloid that mimics the features of in vivo

implantation-window endometrium (Fig. 7). With typical ultra-structures of the implantation window, including pinopodes and cilia, it not only demonstrated hormonal responsiveness and characteristic glycogen secretion functions, but also recapitulated the processes such as decidualization, metabolic changes and EMT, while retaining the potential for embryo implantation. This receptive endometrial assembloid serves as a platform to investigate peri-implantation endometrial physiology and pathology, maternal-fetal interactions, with potential practical applications and clinical translation.

Materials and Methods

Establishment of endometrial assembloids

All experiments involving human subjects followed medical ethical principles and the Declaration of Helsinki, and were approved by the Ethics Committee of Qilu Hospital of Shandong University. Informed consents were obtained from patients. Females of reproductive age who received hysterectomy for benign diseases were selected for this study. Clinical information of patients providing endometrial tissue was listed in Dataset S1. Experimental procedures are presented in detail in the Supporting Information.

Hormone treatment of endometrial assembloids

The hormone regimen for inducing endometrial secretory phase, as described by Thomas E. Spencer et al (9), consisted of estradiol for 2 days followed by a combination of estradiol (Sigma E2758), medroxyprogesterone acetate (Selleck S2567) and N6,2′-O-dibutyryladenosine 3′,5′-cyclic monophosphate sodium salt (cAMP) (Sigma D0627) for 6 days.

To simulate the endometrium of implantation window, we developed a model by incorporating various pregnancy-related hormones. The hormone regimen included estradiol for the first two days, followed by a combination of estradiol, medroxyprogesterone acetate, cAMP, Human Chorionic Gonadotropin (HCG) (Livzon Pharmaceutical Group Inc), Human Placental Lactogen (HPL) (R&D Systems 5757-PL), and prolactin (Peprotech 100-07) for 6 days. The CTRL group was cultured in ExM without the addition of hormones. (Fig. 1A) (Table S2)

ACKNOWLEDGMENTS

This work was supported by National Natural Science Foundation of China (82192874 to H.Z), the National Key Research and Development Program of China (2021YFC2700301 to K.W), the Basic Science Center Program (31988101 to Z-J.C.), Fundamental Research Funds for the Central Universities(2022JC006 to K.W), the Fundamental Research Funds of Shandong University Taishan Scholars Program of Shandong Province（ts20190988 to H.Z.; tsqn201909194 to K.W）, Innovative research team of high-level local universities in Shanghai (SHSMU-ZLCX20210201 to

K.W).

We sincerely appreciate Prof. Tianqing Li (Kunming University of Science and Technology) and Prof. Shaorong Gao (Tongji University) for insightful comments and discussions.

We are grateful to Guangzhou Genedenovo Biotechnology Co., Ltd for assisting in sequencing and bioinformatics analysis. We also thank to YiKon Medical from China for technological assistance of ERT, Jingjie PTM Biolab (HangZhou) Co., Inc. for proteomics.

Author contributions: H. Zhao, K. Wu and Z.-J.C conceived the project and supervised research. Y. Zhang, R. Zhao and H. Zhao designed the experiments. Y. Zhang and R. Zhao performed the experiments, analyzed and interpreted data. Y. Zhang wrote the manuscript. R. Zhao, Y. Li, B. Liu, and H. Zhao revised the manuscript. P. Liu provided human endometrium samples. C.Yang, J. Song, T. Li, C. Yin, M. Lu, Z. Hou and C. Zhang provided technical support. All authors revised and approved the manuscript.

The authors declare no competing interest.

References

1. Wang W, *et al.* (2020) Single-cell transcriptomic atlas of the human endometrium during the menstrual cycle. *Nat Med* 26(10):1644-1653.
2. Turco MY, *et al.* (2017) Long-term, hormone-responsive organoid cultures of human endometrium in a chemically defined medium. *Nat Cell Biol* 19(5):568-577.
3. Boretto M, *et al.* (2017) Development of organoids from mouse and human endometrium showing endometrial epithelium physiology and long-term expandability. *Development* 144(10):1775-1786.
4. Cindrova-Davies T, *et al.* (2021) Menstrual flow as a non-invasive source of endometrial organoids. *Commun Biol* 4(1):651.
5. Shun Shibata SE, Luis A. E. Nagai, Eri H. Kobayashi, Akira Oike, Norio Kobayashi, Akane Kitamura, Takeshi Hori, Yuji Nashimoto, Ryuichiro Nakato, Hirotaka Hamada, Hirokazu Kaji, Chie Kikutake, Mikita Suyama, Masatoshi Saito, & Nobuo Yaegashi HO, Takahiro Arima (2024) Modeling embryo-endometrial interface recapitulating human embryo implantation. *Sci Adv* 10(8):eadi4819.
6. Cheung VC, *et al.* (2021) Pluripotent stem cell-derived endometrial stromal fibroblasts in a cyclic, hormone-responsive, coculture model of human decidua. *Cell Rep* 35(7):109138.
7. Gong L, *et al.* (2022) Bi-potential hPSC-derived Mullerian duct-like cells for full-thickness and functional endometrium regeneration. *NPJ Regen Med* 7(1):68.
8. Dolat L & Valdivia RH (2021) An endometrial organoid model of interactions between Chlamydia and epithelial and immune cells. *J Cell Sci* 134(5).
9. Harriet C. Fitzgerald PD, Susanta K. Behura, Danny J. Schust, and Thomas E. Spencer (2019) Self-renewing endometrial epithelial organoids of the human uterus. *Proc Natl Acad Sci U S A* (116(46)):23132-23142.
10. Wiwatpanit T, *et al.* (2020) Scaffold-Free Endometrial Organoids Respond to Excess Androgens Associated With Polycystic Ovarian Syndrome. *J Clin Endocrinol Metab* 105(3):769-780.
11. Thomas M Rawlings KM, Deborah M Taylor, Matteo A Molè, Katherine J Fishwick, Maria Tryfonos, Joshua Odendaal, Amelia Hawkes, Magdalena Zernicka-Goetz, Geraldine M Hartshorne, Jan J Brosens, Emma S Lucas (2021) Modelling the impact of decidual senescence on embryo implantation in human endometrial assembloids. *eLife* 2021;10:e69603.
12. Park SR, *et al.* (2021) 3D stem cell-laden artificial endometrium: successful endometrial regeneration and pregnancy. *Biofabrication* 13(4).
13. Park SR, *et al.* (2023) Development of cell-laden multimodular Lego-like customizable endometrial tissue assembly for successful tissue regeneration. *Biomater Res* 27(1):33.
14. Boretto M, *et al.* (2019) Patient-derived organoids from endometrial disease capture clinical heterogeneity and are amenable to drug screening. *Nat Cell Biol* 21(8):1041-1051.
15. Haider S, *et al.* (2019) Estrogen Signaling Drives Ciliogenesis in Human Endometrial Organoids. *Endocrinology* 160(10):2282-2297.
16. Cochrane DR, *et al.* (2020) Single cell transcriptomes of normal endometrial derived organoids uncover novel cell type markers and cryptic differentiation of primary tumours. *J Pathol* 252(2):201-214.

468 17. Bui BN, *et al.* (2020) Organoids can be established reliably from cryopreserved biopsy
469 catheter-derived endometrial tissue of infertile women. *Reprod Biomed Online* 41(3):465-
470 473.
471 18. Fitzgerald HC, Kelleher AM, Ranjit C, Schust DJ, & Spencer TE (2023) Basolateral secretions
472 of human endometrial epithelial organoids impact stromal cell decidualization. *Mol Hum*
473 *Reprod* 29(4).
474 19. Kirkwood PM, *et al.* (2022) Single-cell RNA sequencing and lineage tracing confirm
475 mesenchyme to epithelial transformation (MET) contributes to repair of the endometrium
476 at menstruation. *Elife* 11.
477 20. Paule SG, *et al.* (2021) Podocalyxin is a key negative regulator of human endometrial
478 epithelial receptivity for embryo implantation. *Hum Reprod* 36(5):1353-1366.
479 21. Auriemma RS, *et al.* (2020) The Interplay Between Prolactin and Reproductive System:
480 Focus on Uterine Pathophysiology. *Front Endocrinol (Lausanne)* 11:594370.
481 22. d'Hauterive SP, *et al.* (2022) Human Chorionic Gonadotropin and Early Embryogenesis:
482 Review. *Int J Mol Sci* 23(3).
483 23. Nwabuobi C, *et al.* (2017) hCG: Biological Functions and Clinical Applications. *Int J Mol Sci*
484 18(10).
485 24. Bazer FW, Burghardt RC, Johnson GA, Spencer TE, & Wu G (2018) Mechanisms for the
486 establishment and maintenance of pregnancy: synergies from scientific collaborations.
487 *Biol Reprod* 99(1):225-241.
488 25. Garcia-Alonso L, *et al.* (2021) Mapping the temporal and spatial dynamics of the human
489 endometrium in vivo and in vitro. *Nat Genet* 53(12):1698-1711.
490 26. Rocío Martínez-Aguilar LEK, Jane J Reavey, Hilary O D Critchley and Jacqueline A Maybin
491 (2021) HYPOXIA AND REPRODUCTIVE HEALTH: The presence and role of hypoxia in the
492 endometrium. *Reproduction* (161(1)):F1-F17.
493 27. Fatmous M, Rai A, Poh QH, Salamonsen LA, & Greening DW (2022) Endometrial small
494 extracellular vesicles regulate human trophectodermal cell invasion by reprogramming
495 the phosphoproteome landscape. *Front Cell Dev Biol* 10:1078096.
496 28. Jiang X, *et al.* (2022) Lack of VMP1 impairs hepatic lipoprotein secretion and promotes
497 non-alcoholic steatohepatitis. *J Hepatol* 77(3):619-631.
498 29. Kuo WT, *et al.* (2021) The Tight Junction Protein ZO-1 Is Dispensable for Barrier Function
499 but Critical for Effective Mucosal Repair. *Gastroenterology* 161(6):1924-1939.
500 30. Bissonnette L, *et al.* (2016) Human S100A10 plays a crucial role in the acquisition of the
501 endometrial receptivity phenotype. *Cell Adh Migr* 10(3):282-298.
502 31. Srivastava C, *et al.* (2018) FAT1 modulates EMT and stemness genes expression in hypoxic
503 glioblastoma. *Int J Cancer* 142(4):805-812.
504 32. Liu L, *et al.* (2020) si-SNHG5-FOXF2 inhibits TGF-beta1-induced fibrosis in human
505 primary endometrial stromal cells by the Wnt/beta-catenin signalling pathway. *Stem Cell*
506 *Res Ther* 11(1):479.
507 33. Geng J, Cui C, Yin Y, Zhao Y, & Zhang C (2022) LncRNA NEAT1 affects endometrial
508 receptivity by regulating HOXA10 promoter activity. *Cell Cycle* 21(18):1932-1944.
509 34. Vargas MF, *et al.* (2012) Effect of single post-ovulatory administration of levonorgestrel
510 on gene expression profile during the receptive period of the human endometrium. *J Mol*
511 *Endocrinol* 48(1):25-36.

35. Kinnear S, Salamonsen LA, Francois M, Harley V, & Evans J (2019) Uterine SOX17: a key player in human endometrial receptivity and embryo implantation. *Sci Rep* 9(1):15495.
36. Huang P, *et al.* (2021) SOX4 facilitates PGR protein stability and FOXO1 expression conducive for human endometrial decidualization *Elife* 2022 Mar 4;11:e72073.
37. He A, *et al.* (2021) The role of transcriptomic biomarkers of endometrial receptivity in personalized embryo transfer for patients with repeated implantation failure. *J Transl Med* 19(1):176.
38. Yang Y, *et al.* (2021) SLC25A1 promotes tumor growth and survival by reprogramming energy metabolism in colorectal cancer. *Cell Death Dis* 12(12):1108.
39. Wang C, *et al.* (2019) MITRAC15/COA1 promotes mitochondrial translation in a ND2 ribosome–nascent chain complex. *EMBO reports* 21(1).
40. Itoh Y, *et al.* (2021) Mechanism of membrane-tethered mitochondrial protein synthesis. *Science* 371(6531):846-849.
41. Wang T, *et al.* (2021) C9orf72 regulates energy homeostasis by stabilizing mitochondrial complex I assembly. *Cell Metabolism* 33(3):531-546.e539.
42. Gu XW, *et al.* (2020) ATP mediates the interaction between human blastocyst and endometrium. *Cell Prolif* 53(2):e12737.
43. Efremova M, Vento-Tormo M, Teichmann SA, & Vento-Tormo R (2020) CellPhoneDB: inferring cell-cell communication from combined expression of multi-subunit ligand-receptor complexes. *Nat Protoc* 15(4):1484-1506.
44. Li M, *et al.* (2022) BUB1 Is Identified as a Potential Therapeutic Target for Pancreatic Cancer Treatment. *Front Public Health* 10:900853.
45. Li T, *et al.* (2022) WNT5A Interacts With FZD5 and LRP5 to Regulate Proliferation and Self-Renewal of Endometrial Mesenchymal Stem-Like Cells. *Front Cell Dev Biol* 10:837827.
46. Owusu-Akyaw A, Krishnamoorthy K, Goldsmith LT, & Morelli SS (2019) The role of mesenchymal-epithelial transition in endometrial function. *Hum Reprod Update* 25(1):114-133.
47. Casazza A, *et al.* (2013) Impeding macrophage entry into hypoxic tumor areas by Sema3A/Nrp1 signaling blockade inhibits angiogenesis and restores antitumor immunity. *Cancer Cell* 24(6):695-709.
48. Wang X, *et al.* (2014) Functional role of arginine during the peri-implantation period of pregnancy. I. Consequences of loss of function of arginine transporter SLC7A1 mRNA in ovine conceptus trophectoderm. *FASEB J* 28(7):2852-2863.
49. Robertson SA, Chin PY, Femia JG, & Brown HM (2018) Embryotoxic cytokines-Potential roles in embryo loss and fetal programming. *J Reprod Immunol* 125:80-88.
50. Du L, *et al.* (2021) Single-cell transcriptome analysis reveals defective decidua stromal niche attributes to recurrent spontaneous abortion. *Cell Prolif* 54(11):e13125.
51. Sancakli Usta C, Turan G, Bulbul CB, Usta A, & Adali E (2020) Differential expression of Oct-4, CD44, and E-cadherin in eutopic and ectopic endometrium in ovarian endometriomas and their correlations with clinicopathological variables. *Reprod Biol Endocrinol* 18(1):116.
52. Le Friec G, *et al.* (2012) The CD46-Jagged1 interaction is critical for human TH1 immunity. *Nat Immunol* 13(12):1213-1221.
53. Bielfeld AP, *et al.* (2019) A Proteome Approach Reveals Differences between Fertile

Women and Patients with Repeated Implantation Failure on Endometrial Level(-)Does hCG Render the Endometrium of RIF Patients? *Int J Mol Sci* 20(2).

54. Feng Zhou & Roy S (2015) SnapShot: Motile Cilia. *Cell* 162(1):224-224.

55. Bo Li Y-PY, Yu-Ying He, Chen Liang, Meng-Yuan Li, Ying Wang, Zeng-Ming Yang (2023) IHH, SHH, and primary cilia mediate epithelial-stromalcross-talk during decidualization in mice. *Sci Signal* 16(774):eadd0645.

56. Li B*, et al.* (2022) Primary Cilia Restrain PI3K-AKT Signaling to Orchestrate Human Decidualization. *International Journal of Molecular Sciences* 23(24):15573.

57. Devesa-Peiro A, Sebastian-Leon P, Parraga-Leo A, Pellicer A, & Diaz-Gimeno P (2022) Breaking the ageing paradigm in endometrium: endometrial gene expression related to cilia and ageing hallmarks in women over 35 years. *Hum Reprod* 37(4):762-776.

58. King K*, et al.* (2021) Dynamics of lipid droplets in the endometrium and fatty acids and oxylipins in the uterine lumen, blood, and milk of lactating cows during diestrus. *J Dairy Sci* 104(3):3676-3692.

59. Vilella F, Ramirez LB, & Simon C (2013) Lipidomics as an emerging tool to predict endometrial receptivity. *Fertil Steril* 99(4):1100-1106.

60. Braga D*, et al.* (2019) Lipidomic profile as a noninvasive tool to predict endometrial receptivity. *Mol Reprod Dev* 86(2):145-155.

61. Guo S*, et al.* (2021) Hypoxia and its possible relationship with endometrial receptivity in adenomyosis: a preliminary study. *Reprod Biol Endocrinol* 19(1):7.

62. Chen M*, et al.* (2020) Bioinformatic analysis reveals the importance of epithelial-mesenchymal transition in the development of endometriosis. *Sci Rep* 10(1):8442.

63. Gjorevski N*, et al.* (2022) Tissue geometry drives deterministic organoid patterning. *Science* 375(6576):eaaw9021.

Figure 1

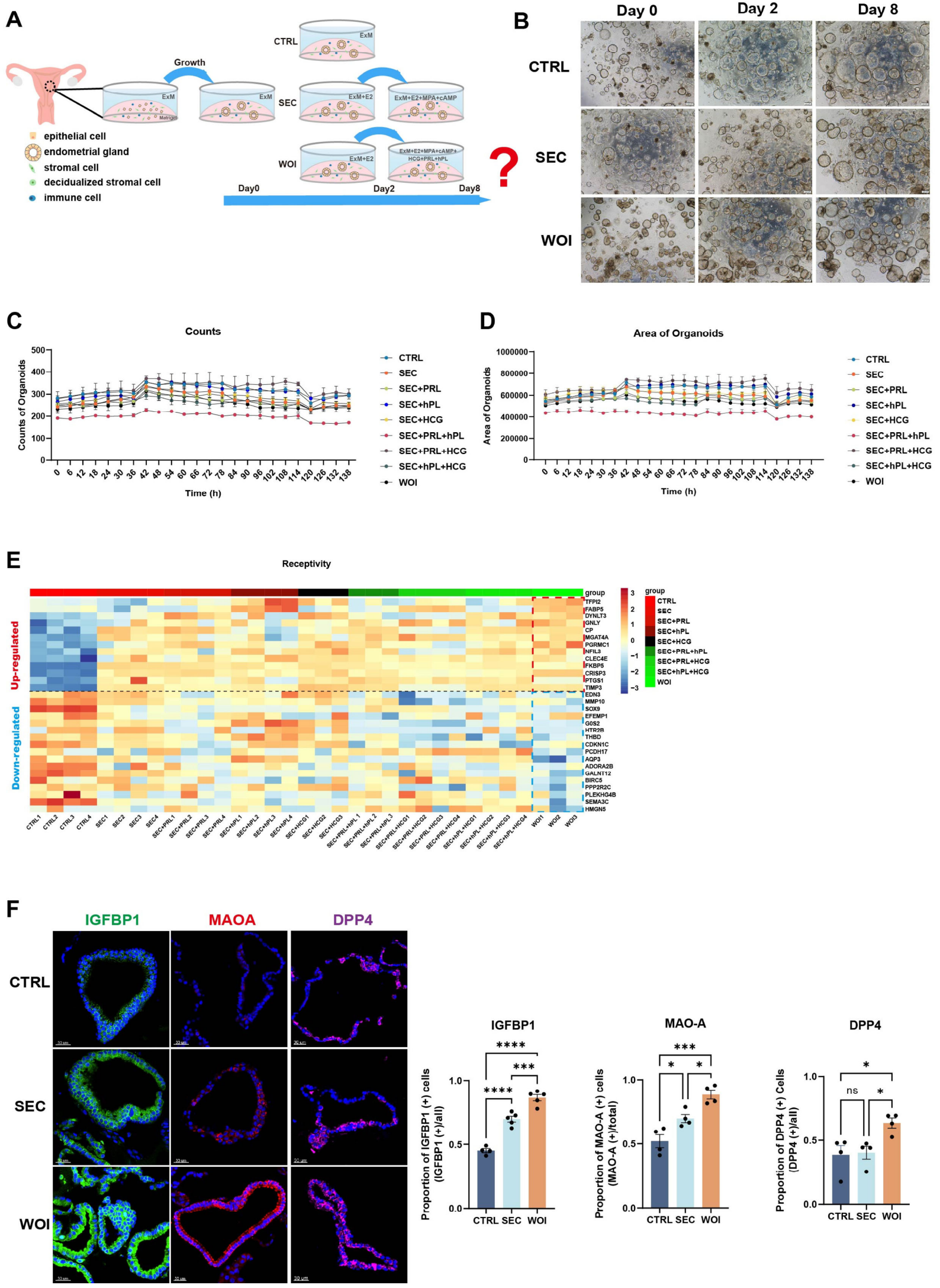
A
CTRL
SEC
WOI
Growth
ExM
Matrigel
ExM+E2
ExM+E2+MPA+cAMP
ExM+E2+MPA+cAMP+ HCG+PRL+hPL
epithelial cell
endometrial gland
stromal cell
decidualized stromal cell
immune cell
Day0
Day2
Day8
B
Day 0
Day 2
Day 8
C
Counts
Counts of Organoids
Time (h)
D
Area of Organoids
Area of Organoids
Time (h)
CTRL
SEC
SEC+PRL
SEC+hPL
SEC+HCG
SEC+PRL+hPL
SEC+PRL+HCG
SEC+hPL+HCG
WOI
E
Receptivity
Up-regulated
Down-regulated
group
TFPI2
FABP5
DYNLT3
GNLY
CP
MGAT4A
PGRMC1
NFIL3
CLEC4E
FKBP5
CRISP3
PTGS1
TIMP3
EDN3
MMP10
SOX9
EFEMP1
G0S2
HTR2B
THBD
CDKN1C
PCDH17
AQP3
ADORA2B
GALNT12
BIRC5
PPP2R2C
PLEKHG4B
SEMA3C
HMGN5
F
IGFBP1
MAOA
DPP4
IGFBP1
MAO-A
DPP4
Proportion of IGFBP1 (+) cells (IGFBP1 (+)/all)
Proportion of MAO-A (+) cells (MAO-A (+)/total)
Proportion of DPP4 (+) Cells (DPP4 (+)/all)
CTRL SEC WOI
ns

Fig 1 Developing receptive endometrial assembloids in vitro

(A) Human endometrial assembloids constructed from adult stem cells were treated with expansion medium (ExM) (CTRL) or subjected to hormonal stimulation. Timeline of endometrial assembloid cultured by ExM (CTRL), ovarian steroid hormones simulating secretory phase (SEC), ovarian steroid hormones combining PRL and placental hormones to mimic the window of implantation (WOI).

(B) Endometrial assembloids in the CTRL, SEC and WOI groups displayed similar growth patterns during the culture period. Scale bar = 200 μm.

(C) The dynamic changes of the counts of assembloids over time in each hormone regimen.

(D) The dynamic changes of the area of assembloids over time in each hormone regimen.

(E) Heatmap showing receptivity related gene expression profile of assembloids in each hormone regimen. The color represents log-transformed fold change of gene expression.

(F) Validation of receptivity markers (IGFBP1, MAOA and DPP4) with immunofluorescence (IF) in the CTRL, SEC and WOI endometrial assembloids in vitro. Nuclei were counterstained with DAPI. Scale bar = 30 μm. The bar chart displaying the quantitative comparison of receptivity markers among three groups. *$P \leq 0.05$, **$P \leq 0.005$, ***$P \leq 0.0005$, ****$P \leq 0.0001$.

Figure 2

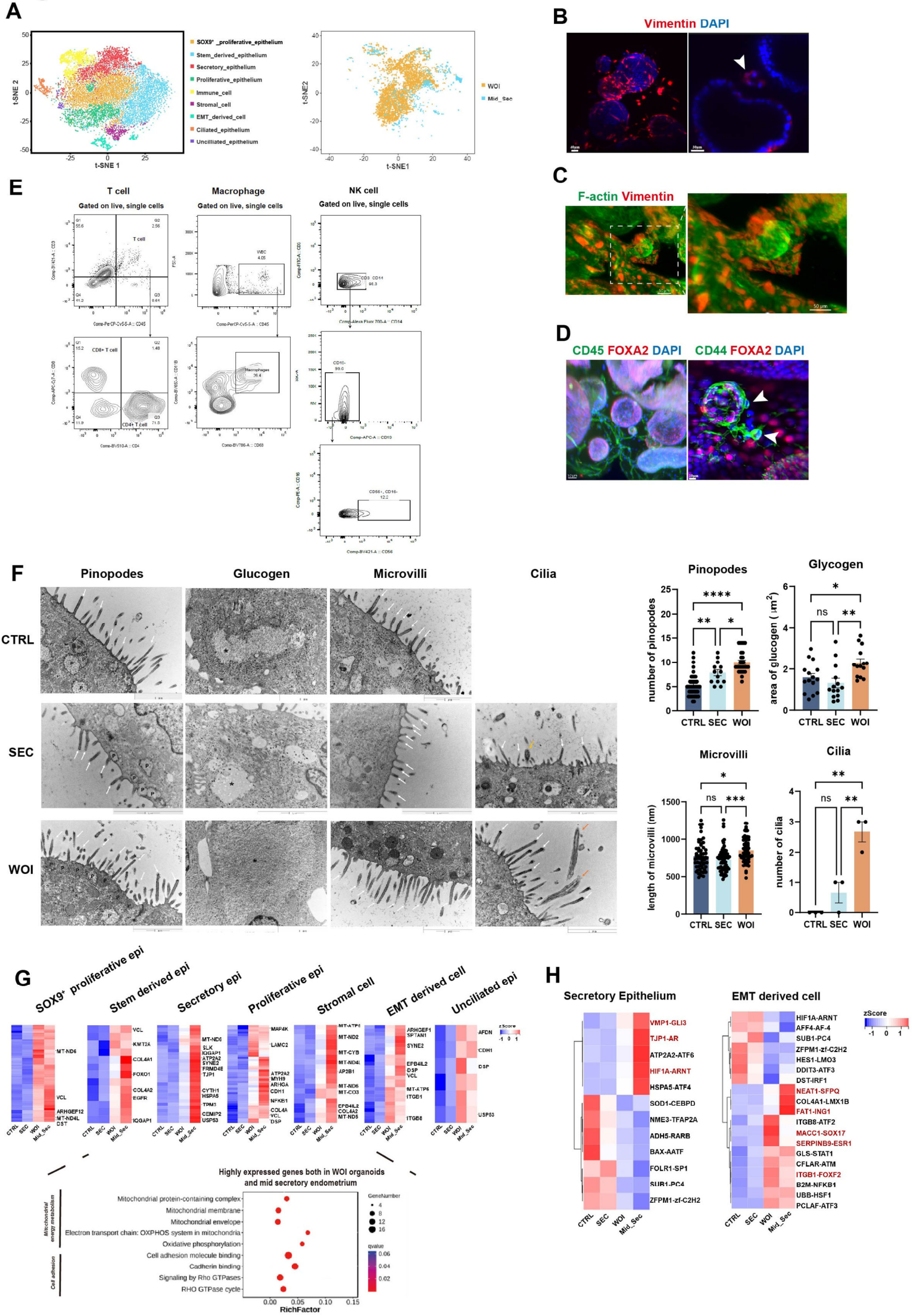
A
t-SNE 1
t-SNE 2
SOX9⁺ _proliferative_epithelium
Stem_derived_epithelium
Secretory_epithelium
Proliferative_epithelium
Immune_cell
Stromal_cell
EMT_derived_cell
Ciliated_epithelium
Unciliated_epithelium
t-SNE1
t-SNE2
WOI
Mid_Sec
B
Vimentin DAPI
C
F-actin Vimentin
D
CD45 FOXA2 DAPI
CD44 FOXA2 DAPI
E
T cell
Gated on live, single cells
Macrophage
Gated on live, single cells
NK cell
Gated on live, single cells
F
Pinopodes
Glucogen
Microvilli
Cilia
CTRL
SEC
WOI
Pinopodes
number of pinopodes
Glycogen
area of glucogen (μm²)
Microvilli
length of microvilli (nm)
Cilia
number of cilia
CTRL SEC WOI
G
SOX9⁺ proliferative epi
Stem derived epi
Secretory epi
Proliferative epi
Stromal cell
EMT derived cell
Unciliated epi
zScore
Highly expressed genes both in WOI organoids and mid secretory endometrium
Mitochondrial energy metabolism
Cell adhesion
Mitochondrial protein-containing complex
Mitochondrial membrane
Mitochondrial envelope
Electron transport chain: OXPHOS system in mitochondria
Oxidative phosphorylation
Cell adhesion molecule binding
Cadherin binding
Signaling by Rho GTPases
RHO GTPase cycle
GeneNumber
qvalue
RichFactor
H
Secretory Epithelium
EMT derived cell
zScore
VMP1-GLI3
TJP1-AR
ATP2A2-ATF6
HIF1A-ARNT
HSPA5-ATF4
SOD1-CEBPD
NME3-TFAP2A
ADH5-RARB
BAX-AATF
FOLR1-SP1
SUB1-PC4
ZFPM1-zf-C2H2
HIF1A-ARNT
AFF4-AF-4
SUB1-PC4
ZFPM1-zf-C2H2
HES1-LMO3
DDIT3-ATF3
DST-IRF1
NEAT1-SFPQ
COL4A1-LMX1B
FAT1-ING1
ITGB8-ATF2
MACC1-SOX17
SERPINB9-ESR1
GLS-STAT1
CFLAR-ATM
ITGB1-FOXF2
B2M-NFKB1
UBB-HSF1
PCLAF-ATF3
CTRL SEC WOI Mid_Sec

Fig 2 Receptive endometrial assembloids mimicked the implantation - window endometrium

(A) T-SNE plot of scRNA-seq data from three individual endometrial assembloids of the CTRL, SEC and WOI groups (left). T-SNE plot of combined scRNA-seq data from the three kinds of assembloids and mid-secretory endometrium (right).

(B) Exhibition of stromal cell marked by vimentin of CTRL assembloid through whole-mount clearing, immunostaining and light sheet microscopy imaging. Nuclei were counterstained with DAPI. The arrowhead indicates stromal cells. Scale bar = 40 μm (left), Scale bar = 30 μm (right).

(C) Whole-mount immunofluorescence showed that Vimentin$^+$ F-actin$^+$ cells (stromal cells) were arranged around the glandular spheres that were only F-actin$^+$. Scale bar = 50 μm.

(D) Exhibition of immune cell marked by CD45 and CD44, and endometrial gland marked by FOXA2 of CTRL assembloid through whole-mount clearing, immunostaining and light sheet microscopy imaging. Nuclei were counterstained with DAPI. The arrowhead indicates immune cells. Scale bar = 50 μm (left), Scale bar = 10 μm (right).

(E) Flow cytometric analysis of T cells and macrophages in the CTRL endometrial assembloid. Gating strategy used for determining white blood cells (WBC) (CD45$^+$ cells), T cells (CD45$^+$CD3$^+$ cells) and macrophages (CD45$^+$CD68$^+$CD11b$^+$ cells).

(F) Electron micrograph of the CTRL (top), SEC (middle) and WOI (bottom) endometrial assembloid showing pinopodes (P), glycogen granule (asterisk), microvilli (white arrows) and cilia (orange arrows). Scale bar = 1 μm. Quantitative comparison of pinopodes, glycogen, microvilli, and cilia in the CTRL, SEC and WOI assembloids. *$P \leq 0.05$, **$P \leq 0.005$, ***$P \leq 0.0005$, ****$P \leq 0.0001$.

(G) Heatmap and bubble diagram illustrating highly expressed genes as well as GO functions enriched in both assembloids during the WOI and mid secretory endometrial tissue in terms of SOX9$^+$ proliferative epithelium, stem-derived epithelium, secretory epithelium, proliferative epithelium, unciliated epithelium, stromal cells and EMT-derived cells. The color of heatmap represents log-transformed fold change of gene expression.

(H) Heatmaps showing differentially expressed TFs of endometrial assembloids and endometrium in the secretory epithelium (left) and EMT-derived cells (right). The color represents log-transformed fold change of gene expression.

Figure 3

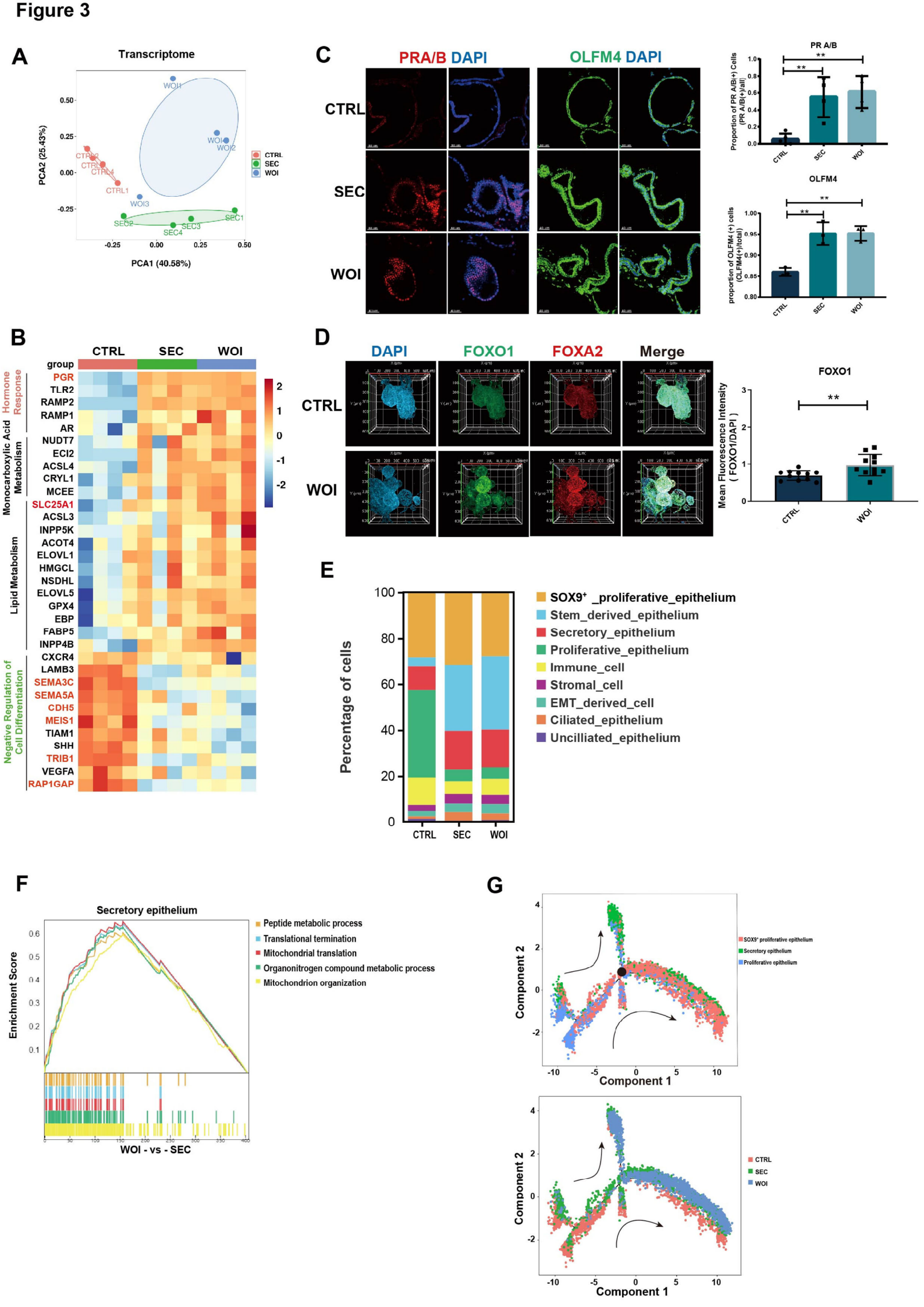
A
Transcriptome
PCA2 (25.43%)
PCA1 (40.58%)
CTRL
SEC
WOI
B
CTRL
SEC
WOI
group
Hormone Response
Monocarboxylic Acid Metabolism
Lipid Metabolism
Negative Regulation of Cell Differentiation
PGR
TLR2
RAMP2
RAMP1
AR
NUDT7
ECI2
ACSL4
CRYL1
MCEE
SLC25A1
ACSL3
INPP5K
ACOT4
ELOVL1
HMGCL
NSDHL
ELOVL5
GPX4
EBP
FABP5
INPP4B
CXCR4
LAMB3
SEMA3C
SEMA5A
CDH5
MEIS1
TIAM1
SHH
TRIB1
VEGFA
RAP1GAP
C
PRA/B DAPI
OLFM4 DAPI
CTRL
SEC
WOI
PR A/B
OLFM4
D
DAPI
FOXO1
FOXA2
Merge
CTRL
WOI
FOXO1
Mean Fluorescence Intensity (FOXO1/DAPI)
E
Percentage of cells
SOX9⁺ _proliferative_epithelium
Stem_derived_epithelium
Secretory_epithelium
Proliferative_epithelium
Immune_cell
Stromal_cell
EMT_derived_cell
Ciliated_epithelium
Uncilliated_epithelium
F
Secretory epithelium
Enrichment Score
Peptide metabolic process
Translational termination
Mitochondrial translation
Organonitrogen compound metabolic process
Mitochondrion organization
WOI - vs - SEC
G
Component 1
Component 2
SOX9⁺ proliferative epithelium
Secretory epithelium
Proliferative epithelium
CTRL
SEC
WOI

Fig 3 Receptive endometrial assembloids recapitulate WOI-associated hormone response

(A) Principal component analysis (PCA) plot computed with differentially expressed genes in the bulk transcriptome of endometrial assembloids belonging to the CTRL, SEC and WOI groups.

(B) Heatmap showing that enrichment of differentially expressed genes for the terms of hormone response, monocarboxylic acid metabolism, lipid metabolism, and negative regulation of cell differentiation. The color represents log-transformed fold change of gene expression.

(C) Responsiveness to progesterone and estrogen was evaluated by IF to PRA/B and OLFM4 with IF respectively. Scale bar = 40 μm, **$P \leq 0.005$.

(D) Exhibition of implantation marker (FOXO1) and endometrial gland marker (FOXA2) through combination of assembloid clearing, IF and light sheet microscopy. Nuclei were counterstained with DAPI. **$P \leq 0.005$.

(E) Bar graph exhibiting various percentages of each cell type in the three groups.

(F) GSEA between the SEC and WOI groups for secretory epithelium.

(G) Pseudotime trajectory showing the transformation between proliferative and secretory epithelium in the CTRL, SEC and WOI groups. Arrows indicate the direction of the pseudotime trajectory. The black dot indicates the key differentiation node.

Figure 4

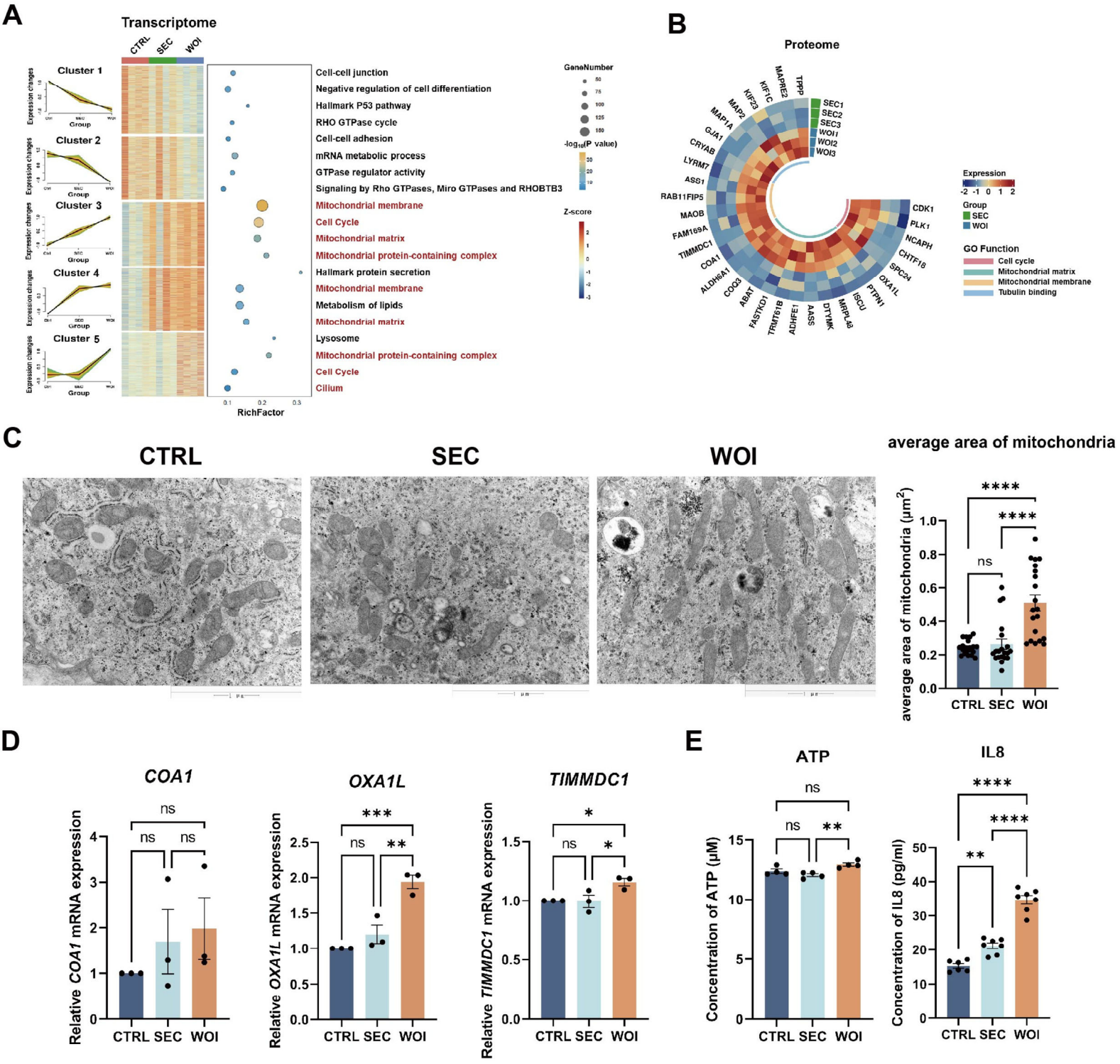
A
Transcriptome
CTRL
SEC
WOI
Cluster 1
Cluster 2
Cluster 3
Cluster 4
Cluster 5
Expression changes
Group
Cell-cell junction
Negative regulation of cell differentiation
Hallmark P53 pathway
RHO GTPase cycle
Cell-cell adhesion
mRNA metabolic process
GTPase regulator activity
Signaling by Rho GTPases, Miro GTPases and RHOBTB3
Mitochondrial membrane
Cell Cycle
Mitochondrial matrix
Mitochondrial protein-containing complex
Hallmark protein secretion
Mitochondrial membrane
Metabolism of lipids
Mitochondrial matrix
Lysosome
Mitochondrial protein-containing complex
Cell Cycle
Cilium
RichFactor
GeneNumber
-log10(P value)
Z-score
B
Proteome
SEC1
SEC2
SEC3
WOI1
WOI2
WOI3
CDK1
PLK1
NCAPH
CHTF18
SPC24
OXA1L
PTPN1
ISCU
MRPL48
DTYMK
AASS
ADHFE1
TRMT61B
FASTKD1
ABAT
COQ3
ALDH6A1
COA1
TIMMDC1
FAM169A
MAOB
RAB11FIP5
ASS1
LYRM7
CRYAB
GJA1
MAP1A
MAP2
KIF23
KIF1C
MAPRE2
TPPP
Expression
Group
SEC
WOI
GO Function
Cell cycle
Mitochondrial matrix
Mitochondrial membrane
Tubulin binding
C
CTRL
SEC
WOI
average area of mitochondria
average area of mitochondria (μm²)
****
****
ns
CTRL SEC WOI
D
COA1
OXA1L
TIMMDC1
Relative COA1 mRNA expression
Relative OXA1L mRNA expression
Relative TIMMDC1 mRNA expression
ns
***
**
*
CTRL SEC WOI
E
ATP
IL8
Concentration of ATP (μM)
Concentration of IL8 (pg/ml)
ns
**
****
CTRL SEC WOI

Fig 4 Receptive endometrial assembloids possess enhanced energy metabolism

(A) The Mfuzz trend analysis displayed the transcriptional variation trends of five clusters from CTRL, SEC, and WOI groups (with a focus on the differences between SEC and WOI assembloids). The heatmap illustrated corresponding gene expression profile (where color represents Z-score). The bubble plot showed the associated GO functions (with bubble size representing the number of genes and bubble color indicating the P value).

(B) The circular heatmap illustrated the functional differences of SEC and WOI assembloids at the proteomic level. The color represents protein expression levels, and the innermost circle color represents GO functions.

(C) Transmission electron microscopy images displayed the mitochondrial morphology of CTRL, SEC, and WOI assembloids, along with a quantitative comparison of mitochondrial area. Scale bar = 1 μm.

(D) RT-qPCR assessed the expression levels of mitochondrial function-related genes in the three assembloid groups.

(E) Quantitative comparison of the concentration of ATP (left) and IL8 (right) released by CTRL, SEC and WOI assembloids.

*P < 0.05，**P < 0.005，***P < 0.0005，****P < 0.0001.

Figure 5

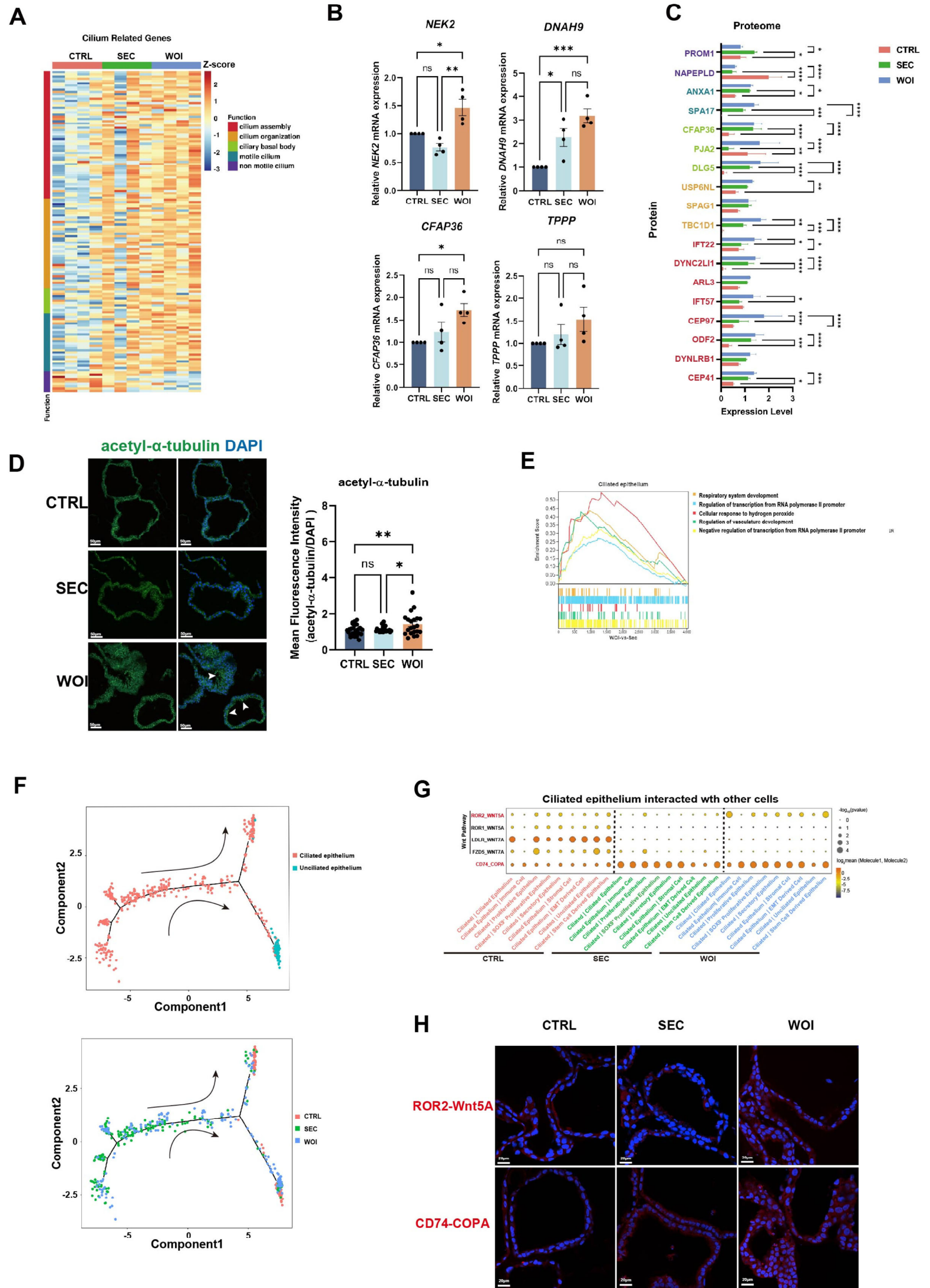
A
Cilium Related Genes
CTRL
SEC
WOI
Z-score
Function
cilium assembly
cilium organization
ciliary basal body
motile cilium
non motile cilium
B
NEK2
DNAH9
CFAP36
TPPP
Relative NEK2 mRNA expression
Relative DNAH9 mRNA expression
Relative CFAP36 mRNA expression
Relative TPPP mRNA expression
ns
C
Proteome
PROM1
NAPEPLD
ANXA1
SPA17
CFAP36
PJA2
DLG5
USP6NL
SPAG1
TBC1D1
IFT22
DYNC2LI1
ARL3
IFT57
CEP97
ODF2
DYNLRB1
CEP41
Protein
Expression Level
D
acetyl-α-tubulin DAPI
CTRL
SEC
WOI
acetyl-α-tubulin
Mean Fluorescence Intensity (acetyl-α-tubulin/DAPI)
E
Ciliated epithelium
Respiratory system development
Regulation of transcription from RNA polymerase II promoter
Cellular response to hydrogen peroxide
Regulation of vasculature development
Negative regulation of transcription from RNA polymerase II promoter
Enrichment Score
WOI-vs-Sec
F
Ciliated epithelium
Unciliated epithelium
Component1
Component2
CTRL
SEC
WOI
G
Ciliated epithelium interacted wth other cells
Wnt Pathway
ROR2_WNT5A
ROR1_WNT5A
LDLR_WNT7A
FZD5_WNT7A
CD74_COPA
H
CTRL
SEC
WOI
ROR2-Wnt5A
CD74-COPA

Fig 5 Receptive endometrial assembloids increased the ciliary assembly and motility

(A) The heatmap illustrated the expression of cilia-related genes across the CTRL, SEC, and WOI assembloids. The color represents Z-score, while the leftmost block indicates various characteristic functions related to cilia.

(B) RT-qPCR assessed the expression levels of cilia-related genes in the three assembloids.

(C) The histogram showed the expression of cilia-related proteins in the three groups of assembloids. The color of the longitudinal protein names corresponds to the color of cilia-related functional blocks in Fig 5A.

(D) IF analysis of cilia assembly marked by acetyl-α-tubulin. Nuclei were counterstained with DAPI. The arrowhead indicates cilia. Scale bar = 50 μm.

(E) GSEA between the SEC and WOI groups for ciliated epithelium.

(F) Pseudotime trajectory showing the transformation between ciliated and unciliated epithelium in the CTRL, SEC and WOI groups. Arrows indicate the direction of the pseudotime trajectory.

(G) Dot plots demonstrating the Cellphone DB analysis of relevant receptors and ligands of ciliated epithelium with other cell types. The size of the dot represents the level of significance. The color of the dot indicates the mean of the average expression level of interacting molecule 1 in ciliated epithelium and molecule 2 in other cell types.

(H) Proximity ligation assay (PLA) validating the interactions of ROR2-Wnt5A and CD74-COPA in the CTRL, SEC and WOI assembloids. Red signals the interaction of two proteins. Nuclei were counterstained with DAPI. Scale bar = 20 μm.

*P < 0.05, **P < 0.005, ***P < 0.0005, ****P < 0.0001.

Figure 6

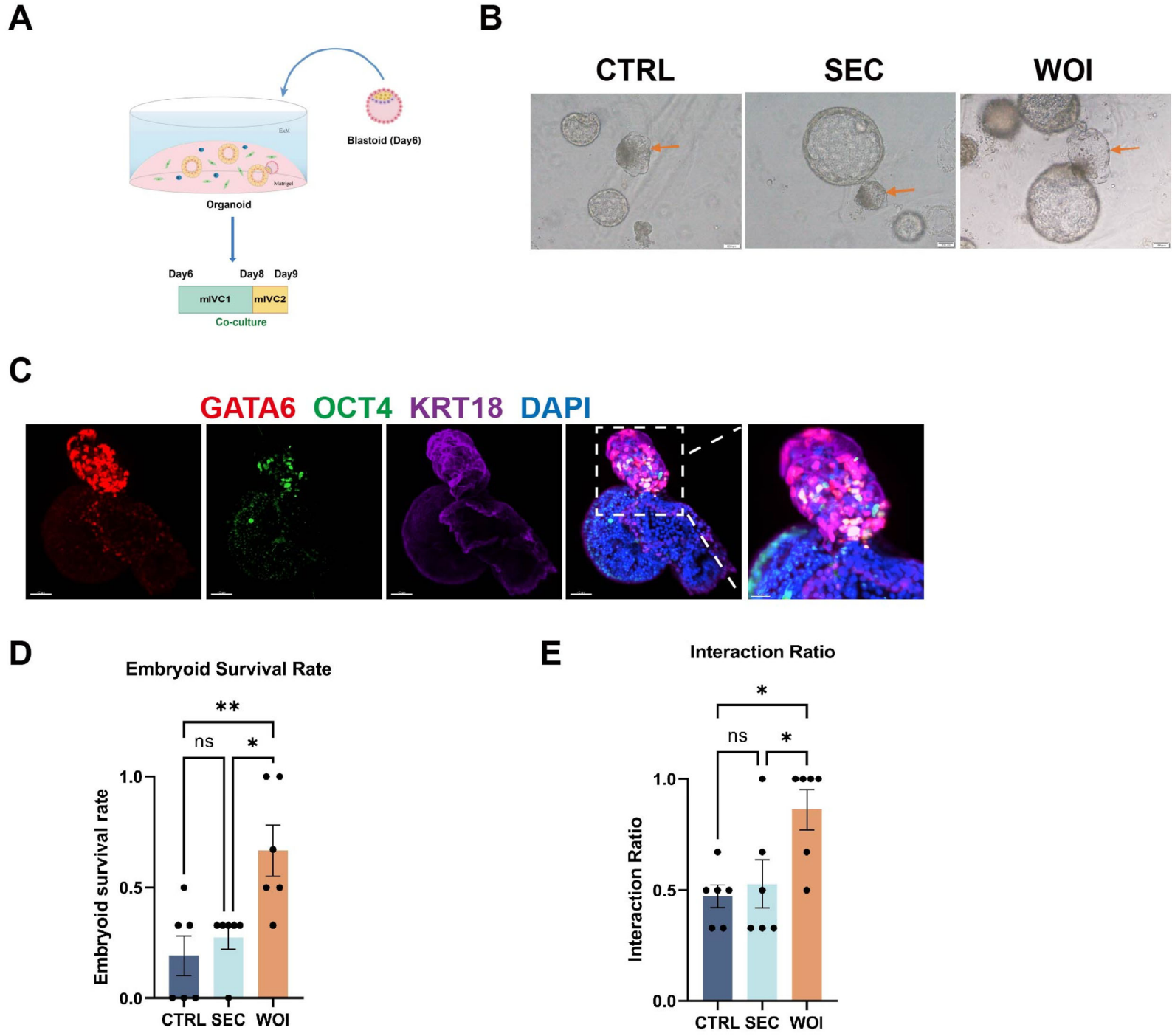
A
Blastoid (Day6)
Organoid
Day6
Day8
Day9
mIVC1
mIVC2
Co-culture
B
CTRL
SEC
WOI
C
GATA6 OCT4 KRT18 DAPI
D
Embryoid Survival Rate
Embryoid survival rate
1.0
0.5
0.0
**
ns
*
CTRL SEC WOI
E
Interaction Ratio
Interaction Ratio
1.0
0.5
0.0
*
ns
*
CTRL SEC WOI

Fig 6 The receptive endometrial assembloids possess the potential for embryo implantation.

(A) Diagram illustrated the co-culture model of endometrial assembloids with blastoids (the blastoid stage corresponds to a 6-day post-fertilization human embryo, referred to as Day 6 here).

(B) Bright-field images of the co-culture of CTRL, SEC, and WOI assembloids with blastoids (Day 9) (yellow arrows indicate the blastoids). Scale bar = 100μm.

(C) Whole-mount fluorescence staining of Day 9 co-cultured embryoid and assembloid. OCT4 indicates the epiblast, GATA6 indicates the hypoblast, and KRT18 indicates the trophoblast. Scale bar = 40μm and 20μm (the rightmost image).

(D) Comparison of the survival rates of Day 9 embryoid in CTRL, SEC, and WOI assembloids.

(E) Comparison of the interaction ratios between Day 9 embryoid and endometrial assembloids in the CTRL, SEC, and WOI groups.

*$P < 0.05$, **$P < 0.005$.

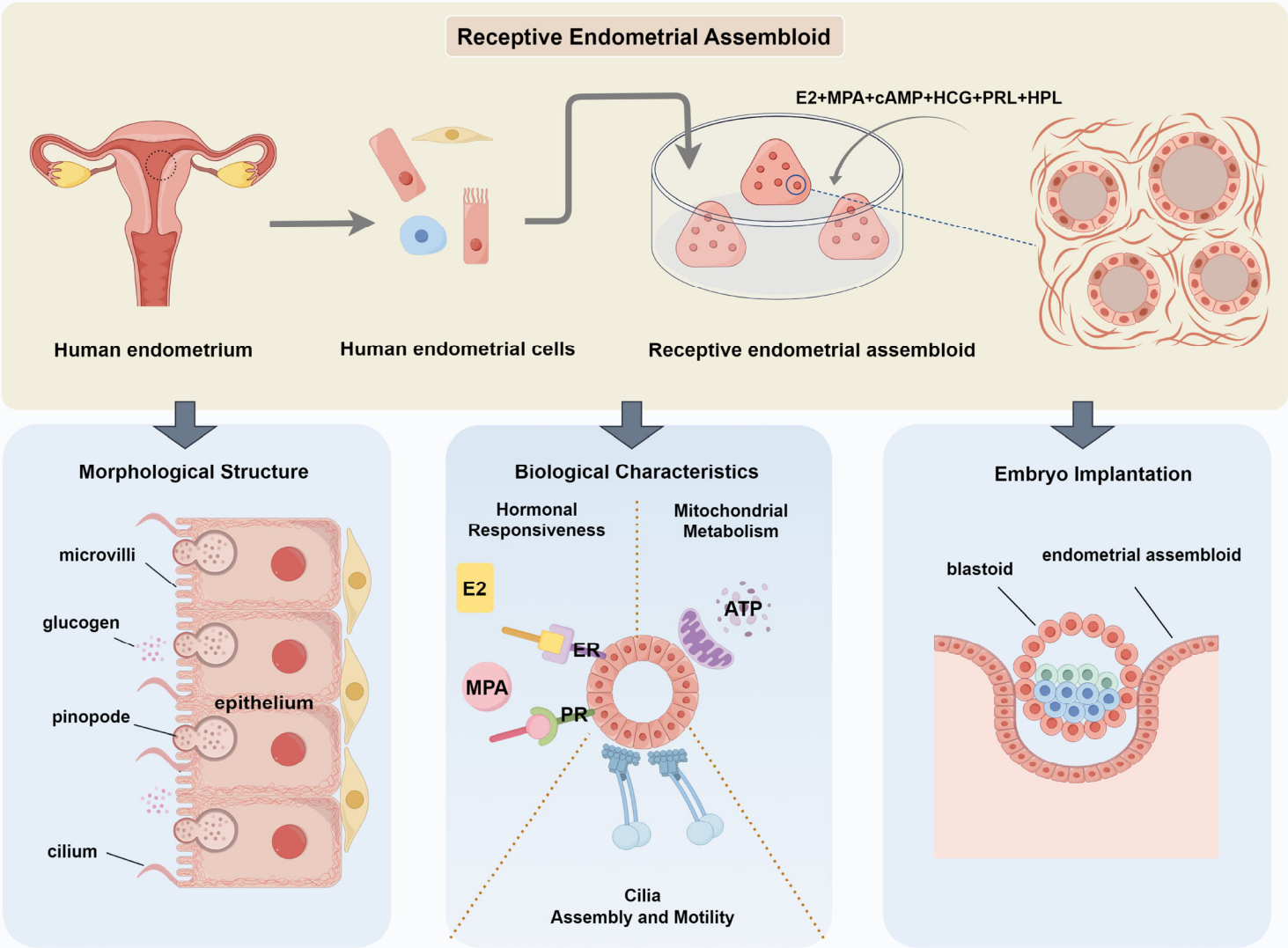
Receptive Endometrial Assembloid
E2+MPA+cAMP+HCG+PRL+HPL
Human endometrium
Human endometrial cells
Receptive endometrial assembloid
Morphological Structure
microvilli
glucogen
pinopode
epithelium
cilium
Biological Characteristics
Hormonal Responsiveness
Mitochondrial Metabolism
E2
ATP
ER
MPA
PR
Cilia Assembly and Motility
Embryo Implantation
blastoid
endometrial assembloid

Fig.7 Schematic diagram displaying the establishment and validation of receptive endometrial assembloids, and summarizing the characteristic biological events of implantation-window endometrium.

Figure S1

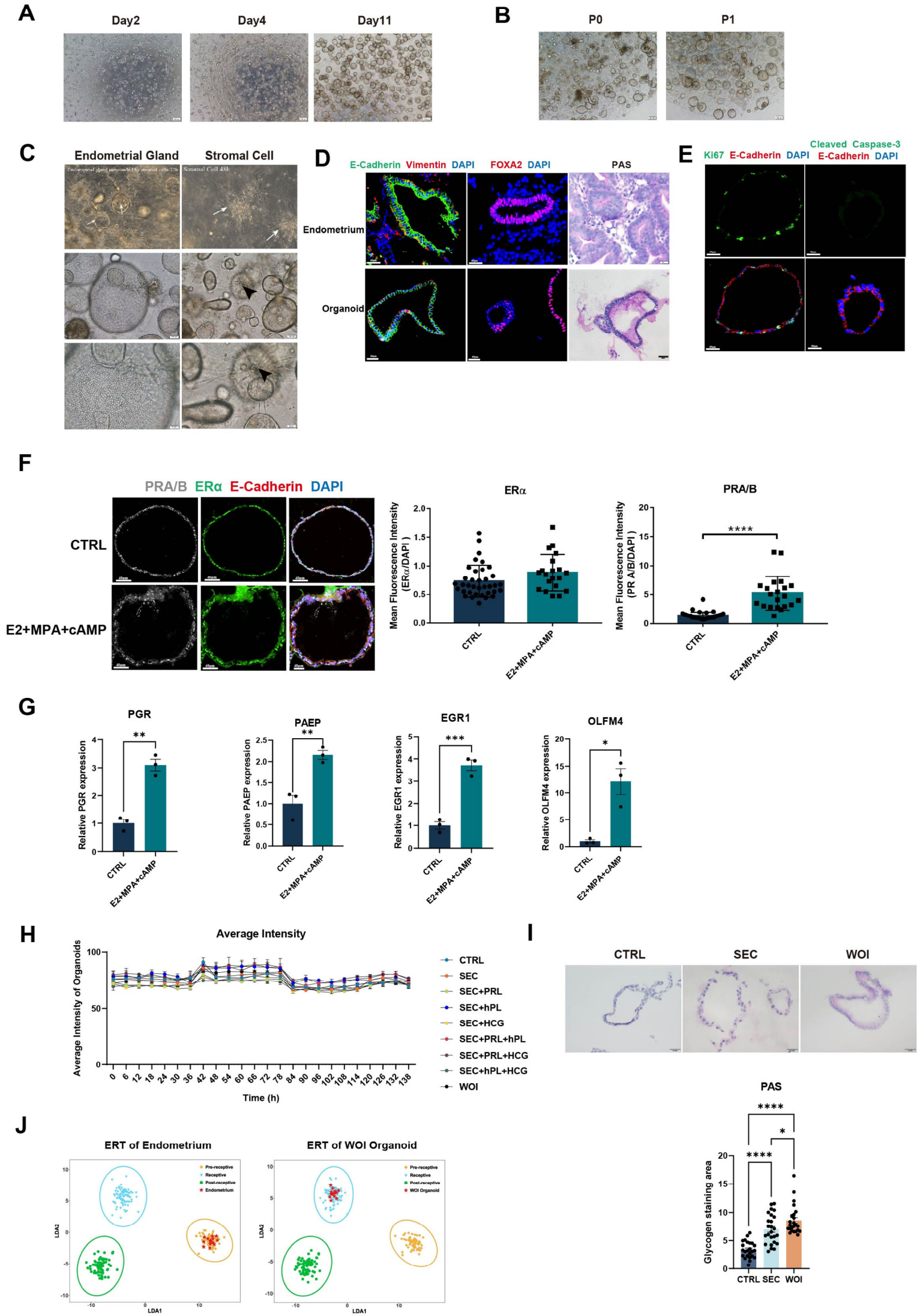
A
Day2
Day4
Day11
B
P0
P1
C
Endometrial Gland
Stromal Cell
D
E-Cadherin Vimentin DAPI
FOXA2 DAPI
PAS
Endometrium
Organoid
E
Ki67 E-Cadherin DAPI
Cleaved Caspase-3 E-Cadherin DAPI
F
PRA/B ERα E-Cadherin DAPI
CTRL
E2+MPA+cAMP
ERα
Mean Fluorescence Intensity (ERα/DAPI)
PRA/B
Mean Fluorescence Intensity (PR A/B/DAPI)
****
G
PGR
Relative PGR expression
PAEP
Relative PAEP expression
EGR1
Relative EGR1 expression
OLFM4
Relative OLFM4 expression
H
Average Intensity
Average Intensity of Organoids
Time (h)
CTRL
SEC
SEC+PRL
SEC+hPL
SEC+HCG
SEC+PRL+hPL
SEC+PRL+HCG
SEC+hPL+HCG
WOI
I
CTRL
SEC
WOI
PAS
Glycogen staining area
J
ERT of Endometrium
Pre-receptive
Receptive
Post-receptive
Endometrium
ERT of WOI Organoid
WOI Organoid
LDA1
LDA2

Fig. S1 Developing receptive endometrial assembloids in vitro

(A) Brightfield of endometrial assembloids on day2, day4 and day11. Scale bar = 200 μm.

(B) Brightfield of endometrial assembloids in the primary generation (P0) and first generation (P1). Scale bar = 200 μm.

(C) Screenshot of video S1 showing endometrial glands gradually developing into a vesicular shape, and the surrounding stromal cells arranging in a fibrous pattern in the CTRL endometrial assembloids (100x, up-left) (The yellow arrows indicate stromal cells and the white arrows indicate endometrial glands). Screenshot of video S2 displaying the stromal cells growing in fibrous pattern and forming an extensive network in the CTRL endometrial assembloids (200x, up-right) (The white arrows indicate stromal cells). The epithelial cells arrange like paving stones (middle and down, left). Stromal cells formed an extensive network (middle and down, right) (The arrowhead indicates stromal cells). Scale bar = 100 μm (middle), Scale bar = 50 μm (down).

(D) Validation of epithelial, stromal cell and endometrial gland markers (E-cadherin, vimentin and FOXA2, respectively) with immunofluorescence (IF) in the endometrium in vivo and CTRL endometrial assembloids in vitro. Nuclei were counterstained with DAPI. Scale bar = 40 μm. Periodic acid-schiff staining (PAS) of endometrium in vivo and endometrial assembloid in vitro. Scale bar = 20 μm.

(E) IF analysis of proliferation and apoptosis indicated by Ki67 and cleaved caspase-3 in the CTRL assembloids, respectively. Nuclei were counterstained with DAPI. Scale bar = 40 μm.

(F) Verification of hormone responsiveness by the expression levels of ERα and PRA/B (E-cadherin indicated the marker of epithelial cell). Scale bar = 40 μm. ***$P \leq 0.0005$.

(G) Relative expression of PGR, PAEP, EGR1, and OLFM4 in the CTRL and hormone-treated assembloids by RT-qPCR. *$P \leq 0.05$, **$P \leq 0.005$, ***$P \leq 0.0005$.

(H) The dynamic changes of the average intensity of assembloids over time in each hormone regimen.

(I) PAS of CTRL, SEC and WOI assembloids. Scale bar = 20 μm. Quantitative comparison of glycogen staining area in the CTRL, SEC and WOI assembloids. *$P \leq 0.05$, ****$P \leq 0.0001$.

(J) Endometrial receptivity evaluation of endometrium and their derived WOI assembloids through ERT. Asterisks indicate individual samples.

Figure S2

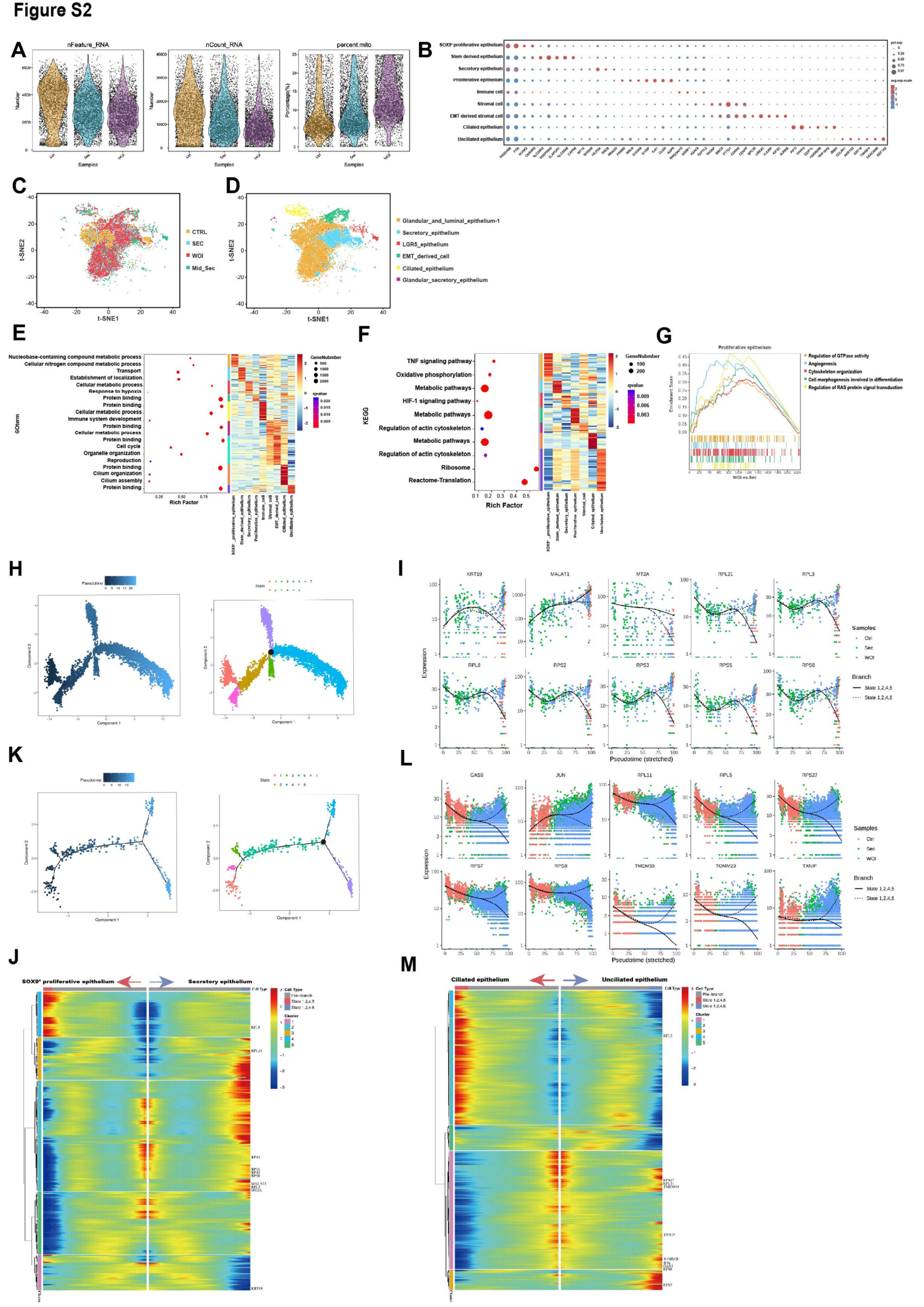
A
nFeature_RNA
nCount_RNA
percent.mito
Samples
B
SOX9+ proliferative epithelium
Stem derived epithelium
Secretory epithelium
Proliferative epithelium
Immune cell
Stromal cell
EMT derived stromal cell
Ciliated epithelium
Unciliated epithelium
C
t-SNE1
t-SNE2
CTRL
SEC
WOI
Mid_Sec
D
Glandular_and_luminal_epithelium-1
Secretory_epithelium
LGR5_epithelium
EMT_derived_cell
Ciliated_epithelium
Glandular_secretory_epithelium
E
GOterm
Nucleobase-containing compound metabolic process
Cellular nitrogen compound metabolic process
Transport
Establishment of localization
Cellular metabolic process
Response to hypoxia
Protein binding
Cellular metabolic process
Immune system development
Cell cycle
Organelle organization
Reproduction
Cilium organization
Cilium assembly
Rich Factor
GeneNubmber
qvalue
F
KEGG
TNF signaling pathway
Oxidative phosphorylation
Metabolic pathways
HIF-1 signaling pathway
Regulation of actin cytoskeleton
Ribosome
Reactome-Translation
Rich Factor
GeneNubmber
qvalue
G
Proliferative epithelium
Enrichment Score
Regulation of GTPase activity
Angiogenesis
Cytoskeleton organization
Cell morphogenesis involved in differentiation
Regulation of RAS protein signal transduction
WOI-vs-Sec
H
Pseudotime
State
Component 1
Component 2
I
KRT19
MALAT1
MT2A
RPL21
RPL3
RPL8
RPS2
RPS3
RPS5
RPS6
Expression
Pseudotime (stretched)
Samples
Ctrl
Sec
WOI
Branch
State 1,2,4,5
State 1,2,4,6
K
Pseudotime
State
Component 1
Component 2
L
GAS5
JUN
RPL11
RPL5
RPS27
RPS7
RPS8
TMEM59
TOMM20
TXNIP
Expression
Pseudotime (stretched)
Samples
Ctrl
Sec
WOI
Branch
State 1,2,4,5
State 1,2,4,6
J
SOX9+ proliferative epithelium
Secretory epithelium
Cell Type
Pre-branch
State 1,2,4,5
State 1,2,4,6
Cluster
RPL8
RPL21
RPS3
RPS5
RPS2
RPS6
MALAT1
RPL3
MT2A
KRT19
M
Ciliated epithelium
Unciliated epithelium
Cell Type
Pre-branch
State 1,2,4,5
State 1,2,4,6
Cluster
RPL5
RPS27
RPL11
TMEM59
TXNIP
TOMM20
JUN
RPL5
RPS8
RPS7

FigS2 Various functions performed by all kinds of cells identified with scRNA-seq.

(A) Box plot of the gene numbers detected, UMI numbers, and ratios of mitochondrial gene expression in single cells of the CTRL, SEC and WOI groups.

(B) Bubble diagram showing the distribution of marker gene expression in each cluster.

(C~D) Comparison of cell composition between CTRL, SEC, WOI endometrial assembloids and mid-secretory endometrium demonstrating samples (C) and cell types (D).

(E) Bubble diagram and heatmap showing the corresponding upregulated genes and GO function of each cluster of endometrial cells.

(F) Bubble diagram and heatmap showing corresponding upregulated genes and KEGG functions of $SOX9^+$ proliferative epithelium, stem-derived epithelium, secretory epithelium, proliferative epithelium, stromal cells, ciliated epithelium and unciliated epithelium. Color is proportional to log-transformed fold change of gene expression.

(G) GSEA between the SEC and WOI groups for proliferative epithelium.

(H) The single-cell pseudotime trajectory of $SOX9^+$ proliferative epithelium, secretory epithelium and proliferative epithelium. Cells start at proliferative epithelium and progress to $SOX9^+$ proliferative epithelium and secretory epithelium (left). There are seven major states over pseudotime (right). The black spot indicates the differentiation node between state 5 and state 6, indicating the direction from proliferative epithelium to $SOX9^+$ proliferative epithelium and secretory epithelium, respectively.

(I)(L) The horizontal axis is the pseudotime point, and the vertical axis is the gene expression level. The solid line represents states 1, 2, 4, and 5 corresponding to Fig. S2H (I) or Fig. S2K (L). Different colors represent samples in the CTRL, SEC and WOI groups.

(J)(M) Heatmap of genes at the branch node regulating differentiation into $SOX9^+$ proliferative epithelium or secretory epithelium (J), and ciliated epithelium or unciliated epithelium (M). The horizontal axis is the pseudo-time point (the pseudo-time point gradually increases from the middle to both sides). The vertical axis is the gene expression level, representing two differential directions on the left and right sides. Clusters represent the gene sets with a similar branch gene expression trend. Different colors represent the level of gene expression.

(K) Pseudotime trajectory of ciliated and unciliated epithelium. Cells start at ciliated epithelium and progress to unciliated epithelium (left). There are seven major states over pseudotime (right). The

black spot indicates the differentiation node between state 5 and state 6, indicating the direction of ciliated and unciliated epithelium, respectively. Arrows indicate the direction of the pseudotime trajectory.

Figure S3

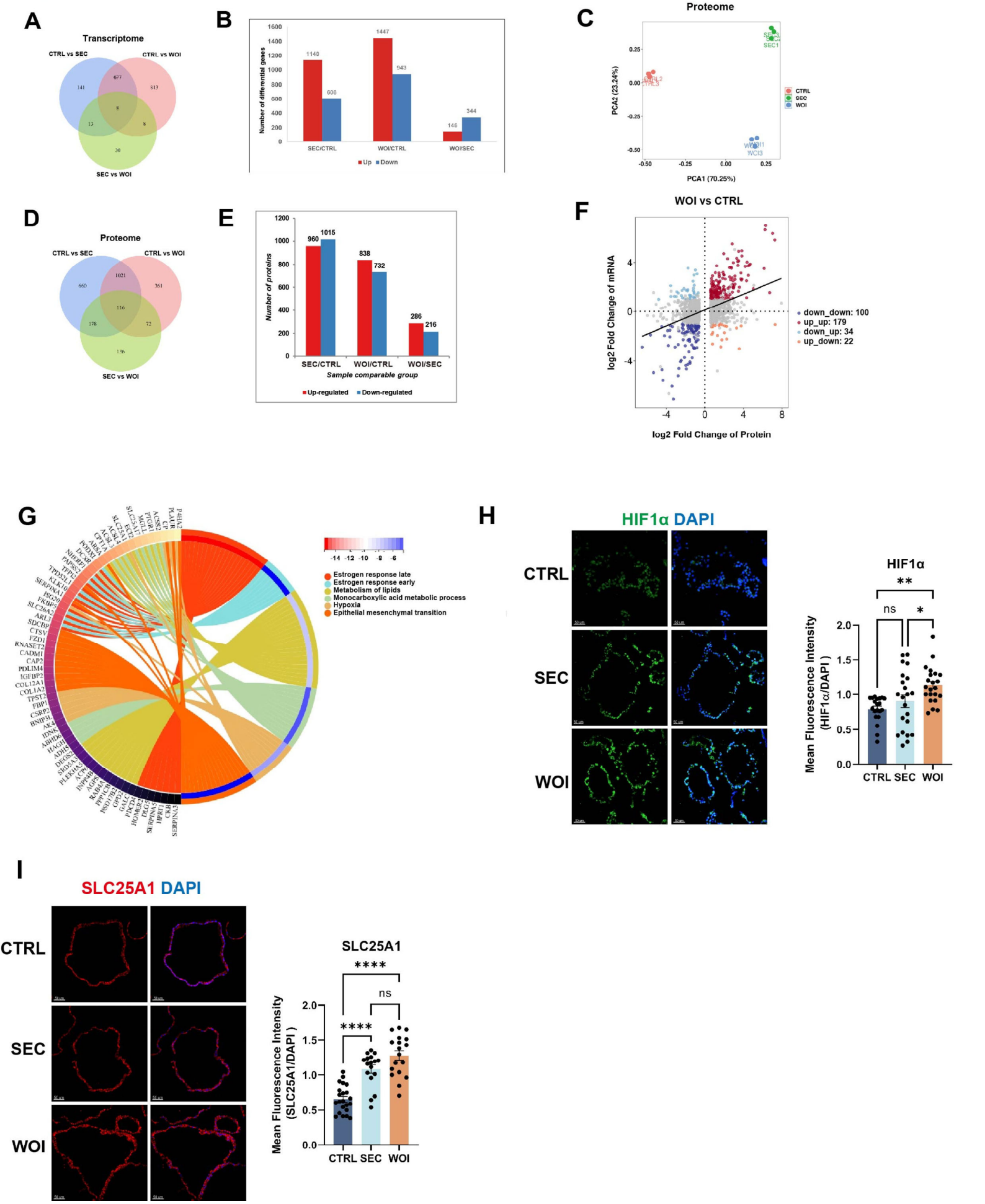
A
Transcriptome
CTRL vs SEC
CTRL vs WOI
SEC vs WOI
141
677
813
8
13
8
20
B
Number of differential genes
1140
608
1447
943
146
344
SEC/CTRL
WOI/CTRL
WOI/SEC
Up
Down
C
Proteome
PCA2 (23.24%)
PCA1 (70.25%)
SEC1
SEC2
SEC3
CTRL1
CTRL2
CTRL3
WOI1
WOI2
WOI3
CTRL
SEC
WOI
D
Proteome
CTRL vs SEC
CTRL vs WOI
SEC vs WOI
660
1021
361
116
178
72
136
E
Number of proteins
960
1015
838
732
286
216
SEC/CTRL
WOI/CTRL
WOI/SEC
Sample comparable group
Up-regulated
Down-regulated
F
WOI vs CTRL
log2 Fold Change of mRNA
log2 Fold Change of Protein
down_down: 100
up_up: 179
down_up: 34
up_down: 22
G
Estrogen response late
Estrogen response early
Metabolism of lipids
Monocarboxylic acid metabolic process
Hypoxia
Epithelial mesenchymal transition
H
HIF1α DAPI
CTRL
SEC
WOI
HIF1α
ns
*
**
Mean Fluorescence Intensity (HIF1α/DAPI)
CTRL SEC WOI
I
SLC25A1 DAPI
CTRL
SEC
WOI
SLC25A1
****
ns
****
Mean Fluorescence Intensity (SLC25A1/DAPI)
CTRL SEC WOI

Fig S3 Comparisons between CTRL, SEC and WOI assembloids at the level of transcriptome and proteome.

(A) Venn diagram showing differential genes in pairs among the three groups. Log_2 FC (Fold Change) > 1.2 or < -1.2, q value < 0.05.

(B) Histogram showing pairwise comparison of differential gene expression (DEG) from bulk RNA-seq among the CTRL, SEC and WOI groups. qvalue < 0.05, |logFC| > 1.

(C) PCA plot computed with differentially expressed proteins in the micro proteomics of endometrial assembloids belonging to the CTRL, SEC and WOI groups.

(D) Venn diagram showing differential proteins in pairs among the three groups. Log_2 FC > 1.2 or < -1.2, q value < 0.05.

(E) Histogram showing pairwise comparison of differential proteins in micro proteomics among the CTRL, SEC and WOI groups.

(F) Scatterplot depicting the correlation between the transcriptome and proteome as for the WOI group and CTRL group. For transcriptome, FC > 2 and p value < 0.05 were defined as significantly upregulated. For proteome, FC > 1.2 and p value < 0.05 were defined as significantly upregulated.

(G) Circle diagram showing the functions of genes upregulated in both the transcriptome and proteome as for the WOI group compared to CTRL group.

(H) Verification of hypoxia response by the expression levels of HIF1α. Scale bar = 50 μm. *P ≤ 0.05, **P ≤ 0.005.

(I) Verification of lipid metabolism by the expression levels of SLC25A1. Scale bar = 50 μm. ****P ≤ 0.0001.

Figure S4

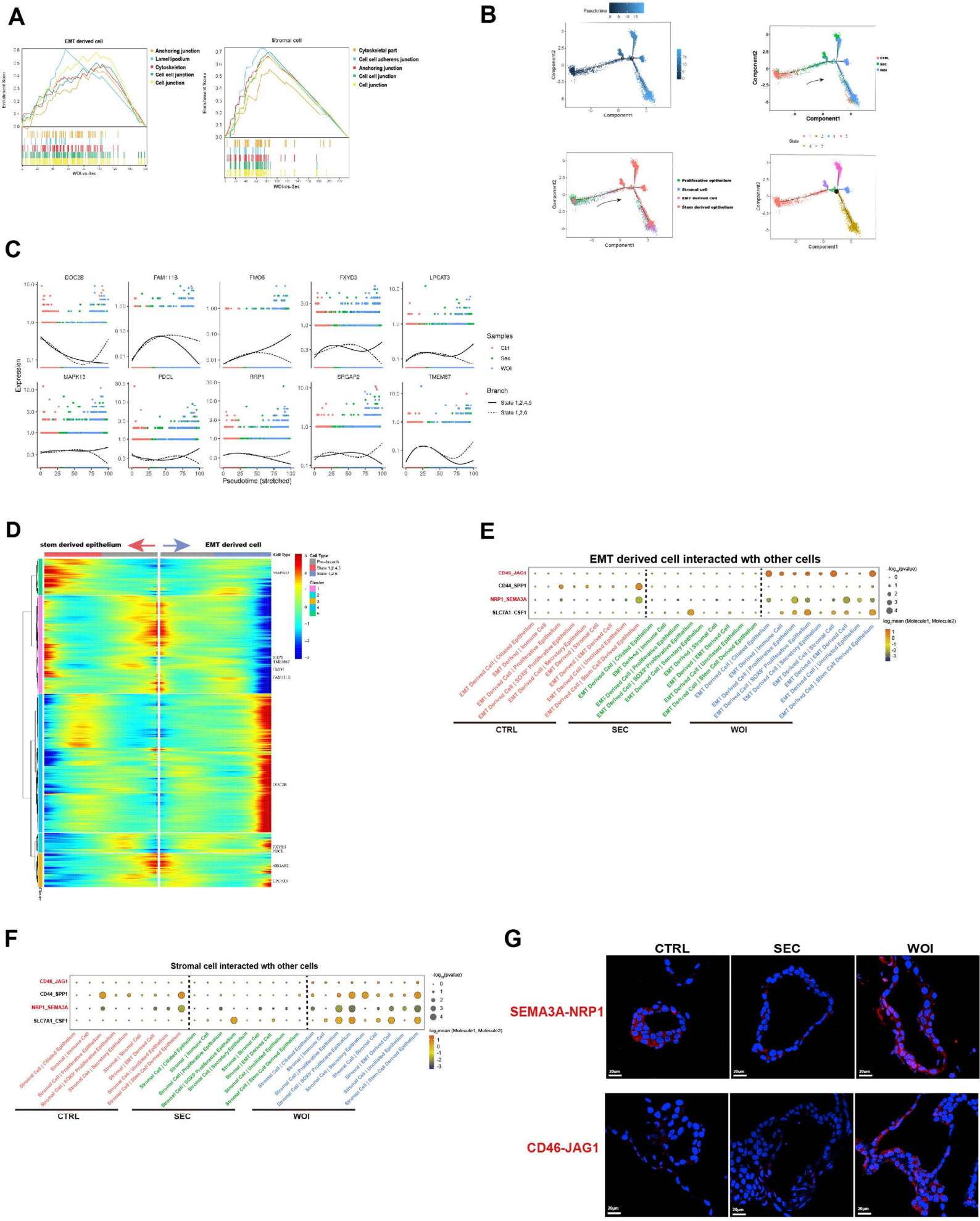
A
EMT derived cell
Anchoring junction
Lamellipodium
Cytoskeleton
Cell cell junction
Cell junction
Stromal cell
Cytoskeletal part
Cell cell adherens junction
Anchoring junction
Cell cell junction
Cell junction
WOI-vs-Sec
B
Pseudotime
Component1
Component2
CTRL
SEC
WOI
State
Proliferative epithelium
Stromal cell
EMT derived cell
Stem derived epithelium
C
DOC2B
FAM111B
FMO5
FXYD3
LPCAT3
MAPK13
PDCL
RRP1
SRGAP2
TMEM87
Expression
Pseudotime (stretched)
Samples
Ctrl
Sec
WOI
Branch
State 1,2,4,5
State 1,2,6
D
stem derived epithelium
EMT derived cell
Cell Type
Pre-branch
State 1,2,4,5
State 1,2,6
Cluster
MAPK13
TMEM
TMEM87
FMO5
FAM111B
DOC2B
FXYD3
PDCL
SRGAP2
LPCAT3
E
EMT derived cell interacted wth other cells
CD46_JAG1
CD44_SPP1
NRP1_SEMA3A
SLC7A1_CSF1
-log10(pvalue)
log2mean (Molecule1, Molecule2)
CTRL
SEC
WOI
F
Stromal cell interacted wth other cells
CD46_JAG1
CD44_SPP1
NRP1_SEMA3A
SLC7A1_CSF1
-log10(pvalue)
log2mean (Molecule1, Molecule2)
CTRL
SEC
WOI
G
CTRL
SEC
WOI
SEMA3A-NRP1
CD46-JAG1
20μm

Fig S4 Receptive endometrial assembloids experienced epithelial-mesenchymal transition (EMT)

(A) GSEA between the SEC and WOI groups for proliferative epithelium.

(B) The single-cell pseudotime trajectory of proliferative epithelium, stromal cell, EMT derived cell and stem derived epithelium. Cells start at proliferative epithelium and progress to EMT derived cell. There are seven major states over pseudotime. The black spot indicates the differentiation node between state 4, 5 and state 6, indicating the direction from proliferative epithelium to EMT derived cell. Arrows indicate the direction of the pseudotime trajectory.

(C) The horizontal axis is the pseudotime point, and the vertical axis is the gene expression level. The solid line represents states 1, 2, 4, and 5 corresponding to Fig. S4B. Different colors represent samples in the CTRL, SEC and WOI groups.

(D) Heatmap of genes at the branch node regulating differentiation into EMT derived cell and stem-derived epithelium. The horizontal axis is the pseudo-time point (the pseudo-time point gradually increases from the middle to both sides). The vertical axis is the gene expression level, representing two differential directions on the left and right sides. Clusters represent the gene sets with a similar branch gene expression trend. Different colors represent the level of gene expression.

(E-F) Dot plots demonstrating the Cellphone DB analysis of relevant receptors and ligands of EMT derived cell (E) or stromal cell (F) with other cell types. The size of the dot represents the level of significance. The color of the dot indicates the mean of the average expression level of interacting molecule 1 in EMT derived cells (E) or stromal cells (F) and molecule 2 in other cell types.

(H) Proximity ligation assay (PLA) validating the interactions of SEMA3A-NRP1 and CD46-JAG1 in the CTRL, SEC and WOI assembloids. Red signals the interaction of two proteins. Nuclei were counterstained with DAPI. Scale bar = 20 μm.